Geochemistry Geophysics Geosystems G3
AN ELECTRONIC JOURNAL OF THE EARTH SCIENCES
Published by AGU and the Geochemical Society

*Article*
Volume 6, Number 12
31 December 2005
Q12009, doi:10.1029/2005GC001021
ISSN: 1525-2027

# Postglacial eruptive history of the Western Volcanic Zone, Iceland

**John Sinton**
*Department of Geology and Geophysics, University of Hawai'i, 1680 East-West Road, Honolulu, Hawaii 96822, USA (sinton@hawaii.edu)*

**Karl Grönvold**
*Nordic Volcanological Institute, University of Iceland, Askja - Sturlugata 7, 101 Reykjavík, Iceland*

**Kristján Sæmundsson**
*Iceland GeoSurvey, Grensásvegur 9, 108 Reykjavík, Iceland*

[1] New field observations, age constraints, and extensive chemical analyses define the complete postglacial eruptive history of the 170-km-long Western Volcanic Zone (WVZ) of Iceland, the ultraslow-spreading western boundary of the south Iceland microplate. We have identified 44 separate eruptive units, 10 of which are small-volume eruptions associated with the flanking Grímsnes system. Overall chemical variations are consistent with very simplified models of melting of a source approximating primitive mantle composition. The 17 eruptions in the first 3000 years of postglacial time account for about 64% of the total postglacial production and are incompatible-element depleted compared to younger units, consistent with enhanced melting as a consequence of rebound immediately following deglaciation. Steadily declining eruption rates for the last 9000 years also correlate with changes in average incompatible element ratios that appear to reflect continued decline in melting extents to the present day. This result is not restricted to the WVZ, however, and may herald a decline in melting throughout all of western Iceland during later postglacial time. Lavas from the northern part of the WVZ are depleted in incompatible elements relative to those farther south at all times, indicating either a long-wavelength gradient in mantle source composition or variations in the melting process along axis. We find no evidence in the postglacial volcanic record for current failure of the WVZ, despite evidence for continued propagation of the eastern margin of the microplate. The dominance of lava shields in the eruptive history of the WVZ contrasts with the higher number of fissure eruptions in other Icelandic volcanic zones. WVZ shields represent long-duration, low-effusion rate eruptions fed by recharge magma arising out of the mantle. Average effusion rate is the key variable distinguishing shield and fissure eruptions, both within the WVZ and between different volcanic zones. High effusion rate, large-volume eruptions require the presence of large crustal magma reservoirs, which have been rare or absent in the WVZ throughout postglacial time.

**Components:** 21,397 words, 14 figures, 6 tables, 1 dataset.

**Keywords:** Iceland; magmatic processes; mid-ocean ridges; volcanic eruptions.

**Index Terms:** 3035 Marine Geology and Geophysics: Midocean ridge processes; 8414 Volcanology: Eruption mechanisms and flow emplacement.

**Received** 16 May 2005; **Revised** 22 September 2005; **Accepted** 8 November 2005; **Published** 31 December 2005.

Sinton, J., K. Grönvold, and K. Sæmundsson (2005), Postglacial eruptive history of the Western Volcanic Zone, Iceland, *Geochem. Geophys. Geosyst.*, *6*, Q12009, doi:10.1029/2005GC001021.

## 1. Introduction

[2] The nature of volcanic eruptions on mid-ocean ridges has important implications for the size and chemical heterogeneity of magma reservoirs that underlie the ridge axis. For example, the size of individual eruptions, along with the internal chemical heterogeneity of them, can be used to constrain the size of magma reservoirs in the crust and/or upper mantle, as well as the extent to which mantle recharge plays a role in triggering individual eruptive episodes. Variations in the timing, size and chemical heterogeneity of eruptive episodes along-axis has implications for the way in which magma is fed to the axis from the underlying mantle. There are, however, few places where the detailed history of volcanic eruptions for a particular spreading ridge system can be worked out in detail [e.g., *Perfit and Chadwick*, 1998; *Sinton et al.*, 2002]. In contrast to submarine mid-ocean ridges, subaerial exposure of the active spreading segments in Iceland allows detailed geologic mapping and age control on the products of individual eruptions. This is especially true for the latest period of erupted activity since the last major glaciation. Postglacial units can be distinguished relatively easily from earlier units and most geological maps of Iceland [e.g., *Jóhannesson and Sæmundsson*, 1998] make this distinction. Division of the postglacial volcanics into individual eruptive units is less straight forward although several previous studies have identified most of the principal units [e.g., *Jónsson*, 1978; *Kjartansson*, 1983; *Sæmundsson*, 1992, 1995; *Sæmundsson and Einarsson*, 1980; *Torfason et al.*, 1999].

[3] In this paper we report the results of detailed study of the Western Volcanic Zone (WVZ) of Iceland (Figures 1 and 2). We have mapped the total outcrop area of every exposed lava unit erupted in postglacial time along the ~170-km-long WVZ and estimated the original erupted volume of each of them. We have obtained new age constraints from $^{14}$C-dating and tephrochronology that have been incorporated into a time-stratigraphic history for the WVZ. In addition, we have produced approximately 300 new whole rock chemical analyses for major and trace elements (see auxiliary material[1]). The geological, geochronological, and chemical data we have obtained are unprecedented for any significant length of mid-ocean ridge, and allows us to evaluate the long-term temporal and spatial systematics of magmatic processes within the WVZ, as well as the chemical heterogeneity of individual eruptive episodes.

## 2. Tectonic Setting of the Ultraslow-Spreading Western Volcanic Zone

[4] Prior to ~6 Ma, the principal plate boundary in western Iceland was the Snæfellsnes Rift, which connected western Iceland to north Iceland. This earlier rift zone was abandoned 6–7 Ma as the locus of spreading jumped to the east and then propagated to the southwest as the Reykjanes-Langjökull rift zone [*McDougall et al.*, 1977; *Sæmundsson*, 1979; *Jóhannesson*, 1980]. This latter zone is now commonly referred to as the Western Volcanic Zone. From ~6 to 2 Ma, seafloor spreading in Iceland was accommodated along the newly formed WVZ and the northern rift zone (NRZ), although the transverse connection to these two spreading ridges is not well defined. The Eastern Volcanic Zone (EVZ) began forming about 1.5–3 Ma [*Sæmundsson and Jóhannesson*, 1994] by propagation of the northern rift zone to the south. The present configuration in South Iceland is dominated by overlapping of the WVZ and EVZ, which form the western and eastern margins, respectively, of the south Iceland microplate [*Sæmundsson*, 1974] (Figure 1). The northern boundary of the microplate is a non-transform relay zone variably referred to as the Mid-Iceland Zone, the Mid-Iceland Belt, or the Hofsjökull Zone (HZ in Figure 1). The southern boundary of the microplate is a transform structure known as the South Iceland Seismic Zone (SISZ). The NVZ is connected to the submarine Kolbeinsey Ridge by the complex Tjörnes Transform while the WVZ is connected to the obliquely spreading submarine Reykjanes Ridge by the Reykjanes Peninsula extensional transform zone (ETZ) [*Taylor et al.*, 1994].

[5] Continuous GPS monitoring (http://hraun.vedur.is/ja/gps.html) (H. Geirsson et al., Current plate movements in Iceland, submitted to *Journal of Geophysical Research*, 2005) indicates total opening rates across the plate boundary zones of Iceland of ~18–20 mm/yr in accord with the Nuvel-1A model of *DeMets et al.* [1994]. The present partitioning of total seafloor spreading across the south Iceland microplate is not well

[1] Auxiliary material is available at ftp://ftp.agu.org/apend/gc/2005GC001021.

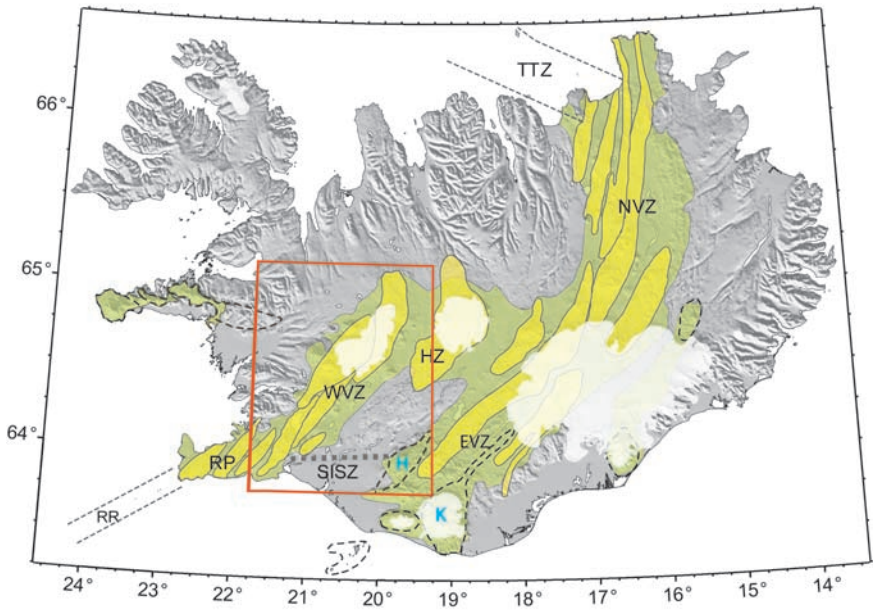


**Figure 1.** Shaded relief map of Iceland. Green regions outline the distribution of upper Pleistocene and Holocene rock units with ages <0.7 Ma [after *Jóhannesson and Saemundsson*, 1998]. The principal volcanic zones defining plate boundaries in Iceland are the Northern Volcanic Zone (NVZ), Eastern Volcanic Zone (EVZ), Hofsjökull Zone (HZ), Western Volcanic Zone (WVZ), and Reykjanes Peninsula (RP). Yellow fields within the volcanic zones are volcanic systems defined by *Einarsson and Sæmundsson* [1987]. Flank volcanic systems are outlined with dashed lines. Flank central volcanoes Hekla (H) and Katla (K) are the sources of ash layers used to constrain eruptive ages in the WVZ. SISZ, South Iceland Seismic Zone; TTZ, Tjörnes Transform Zone; RR, Reykjanes Ridge. Red box outlines the area of Figure 2.

constrained although evidence suggests that the EVZ is opening at a much higher rate than the WVZ. An opening of about 75 m measured across fissures and faults cutting 10,000-year-old lava in the Thingvellir depression [*Bernauer*, 1943] suggests an extension rate of about 5–10 mm/yr along the WVZ. Repeat GPS measurements indicate extension across the WVZ on the order of 3–7 mm/yr [*LaFemina et al.*, 2005]. On the basis of these results, only 20–30% of the total opening across south Iceland is being accommodated along the WVZ, making it the slowest spreading, volcanically active mid-ocean ridge presently recognized, with a rate that qualifies it as an ultraslow spreading center [*Dick et al.*, 2003]. However, unlike submarine ultraslow spreading centers far from hot spots, the WVZ lacks amagmatic accretionary segments. High magma supply associated with the Iceland hot spot results in thicker crust, notably positive relief, and more frequent volcanic activity compared to other spreading centers at comparable spreading rates.

[6] The active volcanic zones within Iceland, including the Reykjanes Peninsula ETZ and various flank zones, can be divided into volcanic systems with each system dominated by a central volcano and associated rift zone or fissure swarm. According to *Einarsson and Sæmundsson* [1987] the WVZ comprises up to four main volcanic systems and a fifth additional flanking system associated with the Grímsnes volcanic field (Figure 1). We discuss the relevance of the concept of volcanic systems to the postglacial volcanic history of the WVZ in a later section.

## 3. Mapping and Stratigraphic Relations

[7] Previous mapping efforts in the Western Volcanic Zone mainly employed hand-specimen examination, tephra stratigraphy, and $^{14}$C-dating of the charred organic remains beneath lava flows. Using these methods, most of the principal postglacial units were defined by the work of *Jakobsson* [1966], *Jónsson* [1978], *Sæmundsson and Einarsson* [1980], *Kjartansson* [1983], *Sæmundsson* [1992, 1995], and *Jóhannesson and Sæmundsson* [1998]. Our new field investigations made only minor modifications to many previously identified boundaries. However, new

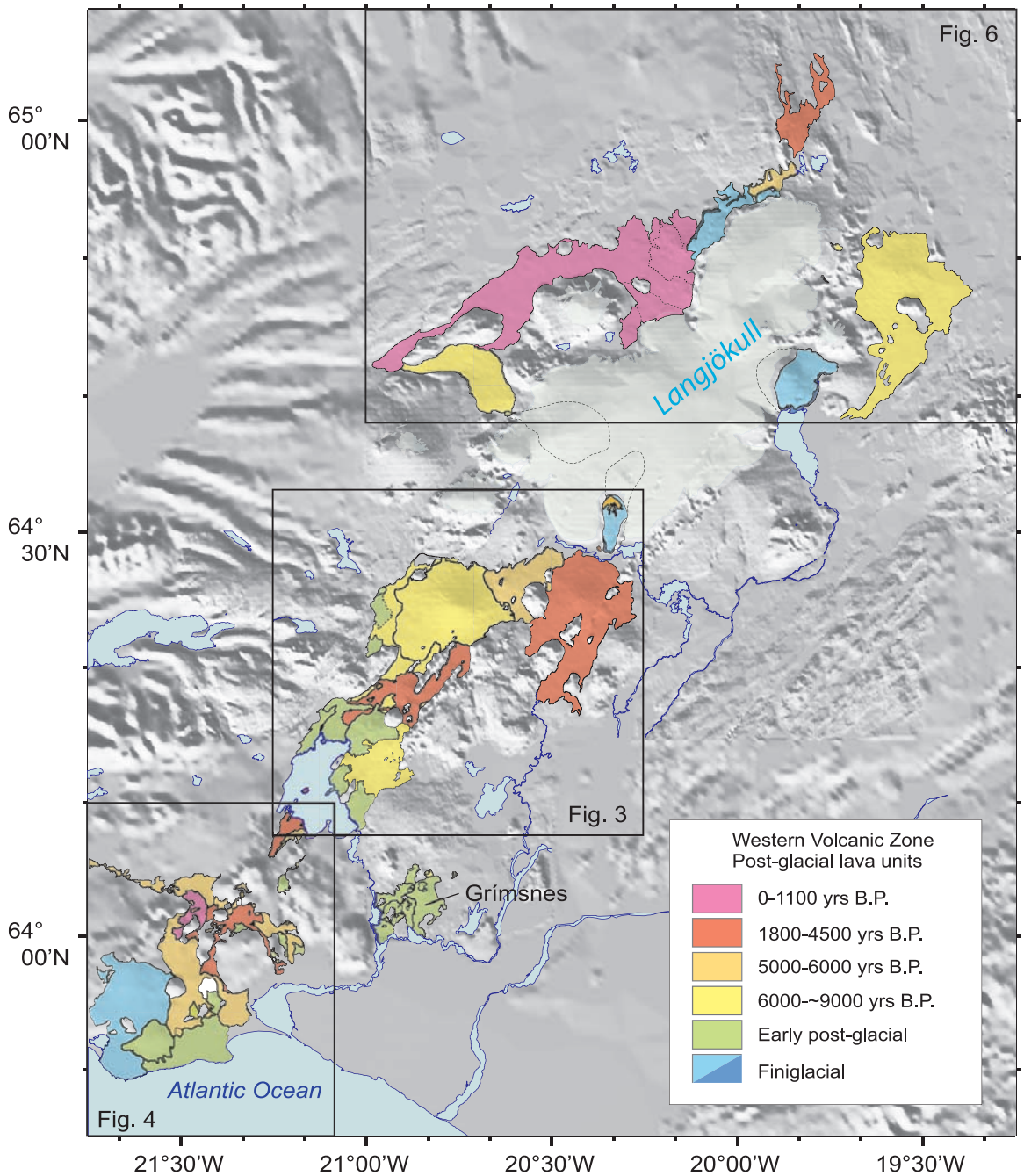


**Figure 2.** Shaded relief map of the Western Volcanic Zone, showing the distribution and age of postglacial lava units (see Table 3 and text for discussion of age control). Rectangles outline the detailed geologic maps of Figures 3, 4, and 6. Dashed contacts extending under Langjökull are based on subglacial topography from data of H. Björnsson (personal communication, 2001). Darker shading on finiglacial units denotes outcrop areas of pillow lava and/or hyaloclastite.

observations of an older shield lava at Hagafell (Figure 3), which had previously been assigned to the last interglacial, indicate that this unit has never been extensively glaciated although a steep flow front composed of pillow lava and hyaloclastite suggest interaction with a thin ice sheet; we therefore assign a finiglacial age to this unit.

[8] The most important contribution of the present study is the incorporation of detailed chemical analyses (see auxiliary material Table 1), which have revealed that some units can be divided into two or more separate eruptive sequences, each showing a distinctive range of chemical composition. The most important example is in the

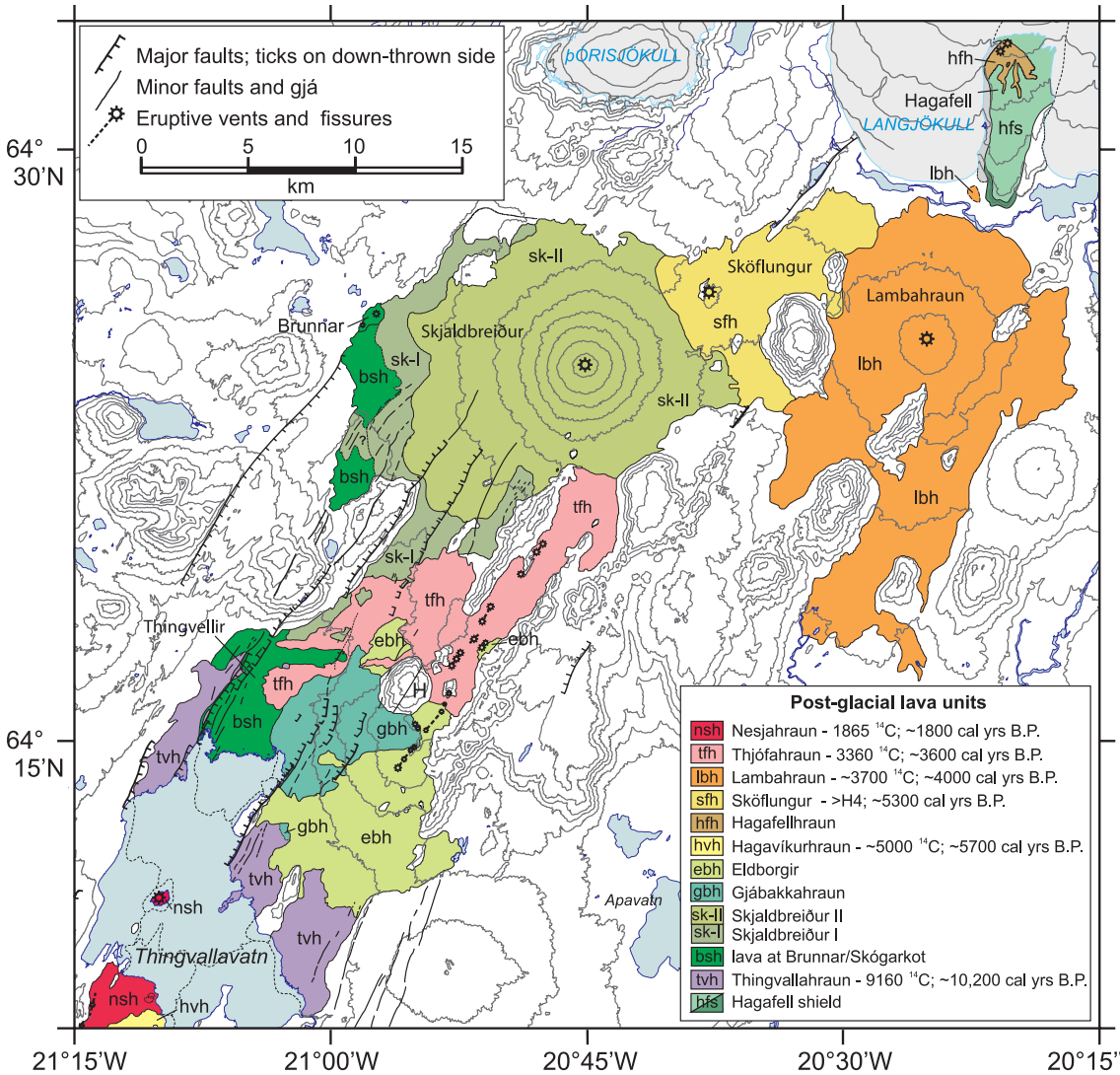


**Figure 3.** Geologic map showing distribution of postglacial lava units and principal faults in the middle part of the WVZ, modified from *Sæmundsson* [1992]. Gjá are open fissures or joints, lacking evidence for eruptive activity. Contacts extending beneath Thingvallavatn are modified after *Thors* [1992] and *Bull et al.* [2003]. H marks the location of Hrafnabjörg table mountain. Topographic contours are in 100 m intervals.

region just north of Thingvallavatn, (Figure 3) where lavas previously designated as Eldborgir by *Saemundsson* [1992], are now considered to comprise four separate eruptive sequences (Thingvallahraun, Brunnar/Skógarkot, Gjábakkahraun, and Eldborgir). Our chemical and stratigraphic data also indicate that lavas in the vicinity of the Skjaldbreiður lava shield can be separated into three chemically distinct units, the oldest of which extends to the northern shores of Thingvallavatn. Our study in this region also has refined contacts between Skjaldbreiður and Sköflungur, and the complete outcrop area of Thjófahraun, which differs from the earlier study of *Sæmundsson* [1992]. Chemical data also have clarified geologic units near the southern end of the WVZ, where we now distinguish the Hafnarhraun, Heiðin há and Selvogsheiði lava shields as chemically distinct, early postglacial lava shields (Figure 4).

[9] In addition to mapping and chemical analysis, we have dated several flow units using accelerator mass spectrometric $^{14}C$ analyses of charcoal remains recovered from beneath lava flows (Table 1), and determined the relationship of several other units to known ash horizons. $^{14}C$ data listed in Table 1 include new charcoal analyses for previously undated Thjófahraun, Lambahraun (2 localities), and Geitlandshraun II units, as well as analyses for the previously dated

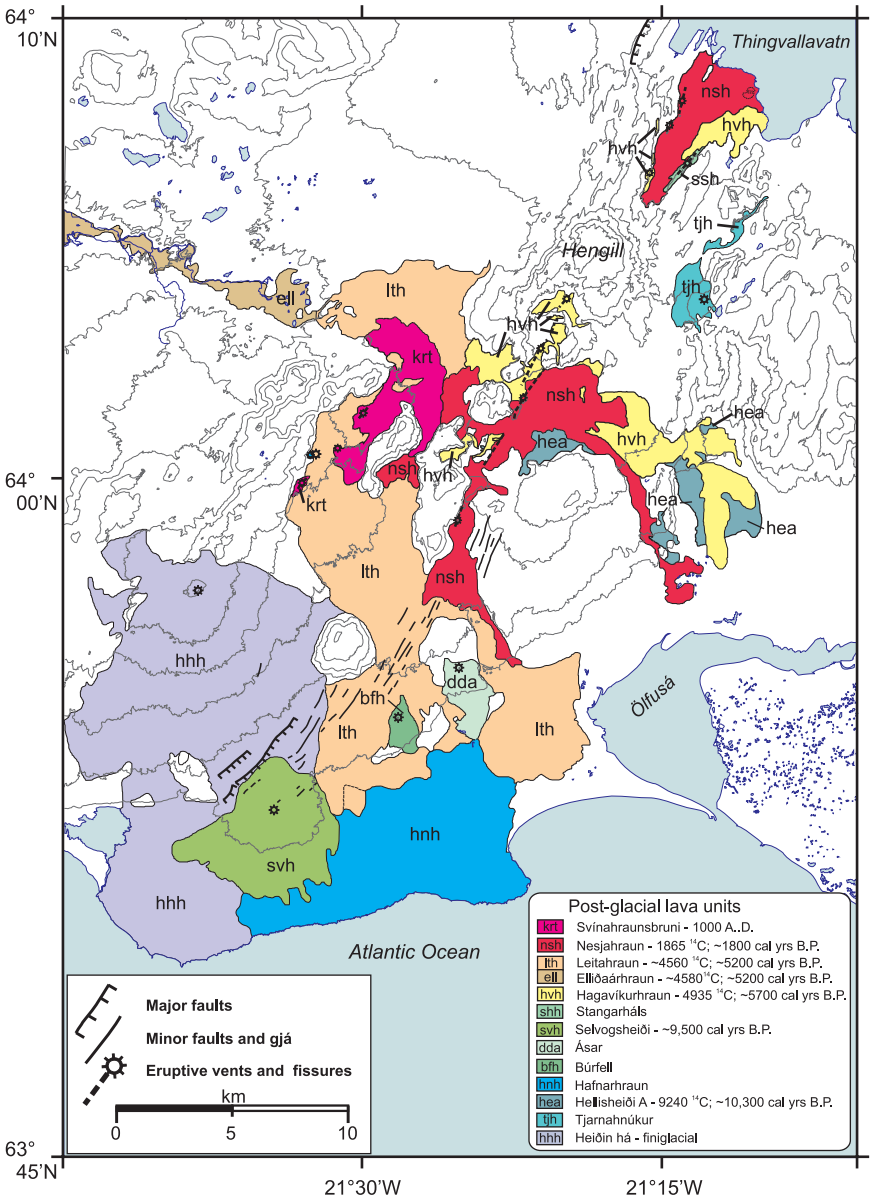


**Figure 4.** Geologic map showing distribution of postglacial lava units in the southern part of the WVZ, modified after *Jónsson* [1978], *Sæmundsson and Einarsson* [1980], and *Sæmundsson* [1995].

lavas of Leitahraun, Hagavíkurhraun, selected lavas within the Grímsnes field, and the Thingvellir lava (Thingvallahraun; hraun = lava in Icelandic). The new age for Thjófahraun is consistent with our observation that the lava lies between two red-brown to black ash layers that probably represent the KE and KN ashes of *Hardardóttir et al.* [2001], with $^{14}$C ages of 2850 ± 10 and 3300 ± 100 years B.P., respectively. The new $^{14}$C age for Lambahraun is consistent with its relationship to the Hekla 3 ash (Figure 5).

[10] Our new data agree with previously published ages for Leitahraun, Hagavíkurhraun (Hellisheiðarhraun B/C) and Thingvallahraun (Table 1). Analysis of charcoal from beneath the lava in Elliðaá valley in Reykjavík, 4580 ± 50, is significantly younger than the first published age of 5300 ± 340 years for this site [*Hospers*, 1953; *Áskelsson*, 1953], but consistent with that obtained by *Jónsson* [1971] from a site close by. Our age agrees with that of stratigraphically younger lavas from Leitin, confirming the interpretation of *Einarsson* [1960] and *Torfason et al.* [1999] that Ellidaáhraun represents an early phase of the Leitin lava shield. Our new age for the Seyðishólar lava at Mýrarkot is significantly older than the age of 6220 ± 140 years B.P. of *Jakobsson* [1976] from

**Table 1.** The $^{14}C$ Ages for Postglacial Western Volcanic Zone Lava Units[a]

| Unit | $^{14}C$ age | Location | Description | Anal. Lab. | Reference |
|---|---|---|---|---|---|
| Hallmundarhraun | | | | | |
| H2453-1857 | 1190 ± 100 | Nordlingafljót | peat beneath lava | U. Heidelberg | *Sæmundsson* [1966] |
| Nesjahraun | | | | | |
| H1716-1240 | 1880 ± 65 | Crater, S. of road, Nesjvellir | carbonized trunks in scoria | U. Heidelberg | *Sæmundsson* [1962] |
| U-4046 | 1860 ± 110 | Hveradalir | | | *Jónsson* [1975] |
| U-2527 | 1855 ± 65 | Hveradalir | | | *Jónsson* [1975] |
| | 2025 ± 65 | Eldborg undir Meitlum | | | *Jónsson* [1983] |
| Thjófahraun | | Söðuholar | carbonized twigs | | |
| IT-278B | 3360 ± 35 | 0506190/7133885 | in ash at base of flow | NOSAMS | this study |
| Lambahraun | | | | | |
| IT-276B | 3550 ± 50 | Hnífagil 0528180/7132330 | charcoal at base of flow | NOSAMS | this study |
| IT-206C | 3830 ± 40 | Thórólfsfell 0523650/7146120 | carbonized sticks in ash at base of flow | NOSAMS | this study |
| Leitahraun | | | | | |
| U-523 | 4530 ± 100 | Hliðardalsskóli | charcoal at base of flow | Inst. Physics, Uppsala | *Kjartansson* [1966a] |
| | 4575 ± 75 | West of Hjalli | charcoal at base of flow | | *Jónsson* [1978] |
| IT-401 | 4550 ± 65 | Hliðardalsskóli 0480763/7088722 | charcoal at base of flow | NOSAMS | this study |
| | 5300 ± 340 | Ellidaá, Reykjavík | | Chicago | *Hospers* [1953]; *Áskelsson* [1953] |
| U-632 | 4630 ± 90 | Ellidaá, Reykjavík | birch charcoal at base of flow | Uppsala | *Jónsson* [1971] |
| IT-332 | 4580 ± 50 | Ellidaá, Reykjavík 0459165/7110636 | charcoal at base of flow | NOSAMS | this study |
| Hagavíkurhraun | | | | | |
| U-2655 | 4935 ± 65 | Hengladalsá | | | *Jónsson* [1977] |
| | 4900 ± 70 | | | | |
| UtC-828 | 4800 ± 130 | | | | *Jónsson* [1989] |
| IT-395 | 5060 ± 55 | Hengladalsá 0487580/7098890 | charcoal at base of flow | NOSAMS | this study |
| IT-396 | 4980 ± 55 | Hengladalsá 0487590/7098860 | charcoal at base of flow | NOSAMS | this study |
| Geitlandshraun II | | Geitá | charcoal at base | | this study |
| IT-268 | 8030 ± 55 | 0513230/7172730 | of flow | NOSAMS | |
| Grímsnes | | | | | |
| K-1166 | 6220 ± 140 | Mýrarkot | | Danish Mus. | *Jakobsson* [1976] |
| AAR-920 | 7400 ± 210 | Borgarhóll | charcoal beneath cinder | U. Aarhus | Sæmundsson and Sveinbjörnsdóttir (unpublished data) |
| IT-294 | 8370 ± 55 | Mýrarkot | charcoal at base of | NOSAMS | this study |
| | 8880 ± 50 | 0510340/7101180 | Seyðishólar flow | | |
| Thingvallahraun | | | | | |
| W-1912 | 9130 ± 260 | Sog | carbonized moss remains below lava | | *Kjartansson* [1964a] |
| IT-413 | 9190 ± 65 | Sog 0498673/7112074 | carbonized moss remains below lava | NOSAMS | this study |
| Hellisheidi A | | | | | |
| UtC-828 | 9240 ± 140 | | | | *Jónsson* [1989] |

[a] All analyses in this study were determined by accelerator mass spectrometry at the NOSAMS (National Ocean Sciences Accelerator Mass Spectrometry) facility at Woods Hole Oceanographic Institution. Ages from this study are reported without reservoir corrections or calibration to calendar years according to the conventions of *Stuiver and Polach* [1977] and *Stuiver* [1980] and are calculated using 5568 years for the half-life of radiocarbon. Locations in UTM coordinates are given for all samples of this study.

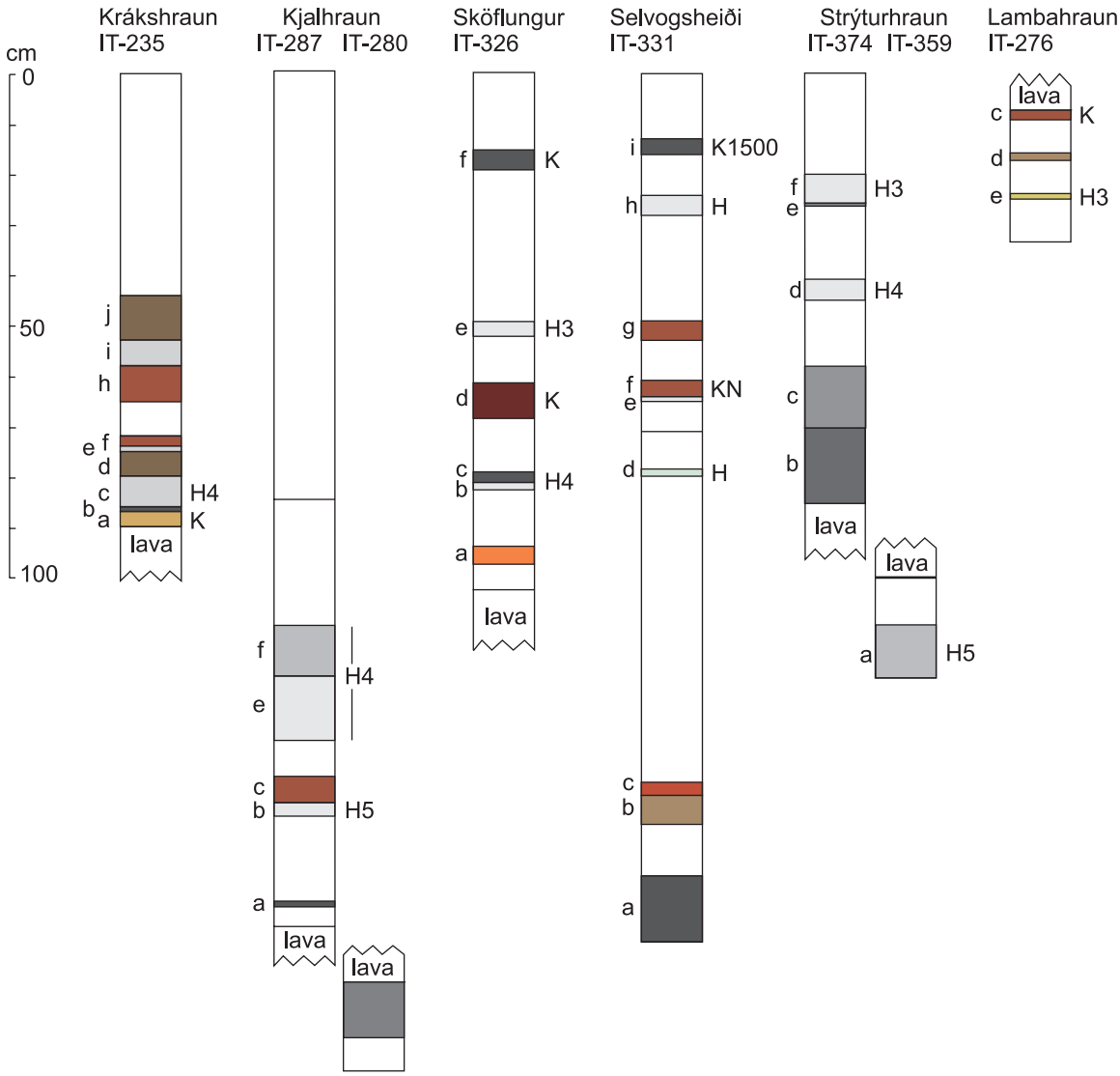


**Figure 5.** Soil profiles showing ash layers on the Krákshraun, Kjalhraun, Sköflungur, Selvogsheiði, and Strýtuhraun lavas, and those underlying Kjalhraun, Strýtuhraun, and Lambahraun. Unpatterned zones are soil horizons; colored zones are ash layers with the color approximating the actual color of the layer; lowercase letters on the left side of each profile correspond to chemical data given in Table 2. Uppercase letters on the right side of each profile show our interpretation of source volcano of selected ashes: H, Hekla; K, Katla (see text for discussion).

the same location. Overall our data suggest that much of the Grímsnes lava field was erupted more than 8000 years ago. Ages referred to hereafter in this paper are corrected to years B.P. (before 1950 A.D.) using the CALIB Radiocarbon Calibration [*Stuiver and Reimer*, 1993], and designated cal. years B.P.

[11] We also have estimated ages for Sköflungur, Strýtuhraun, Krákshraun, Kjalhraun, and Selvogsheiði on the basis of the distribution of ashes in soil profiles (Figure 5). Ash horizons in each soil profile were analyzed by electron microprobe at the University of Iceland (Table 2) and data compared to published and unpublished analyses of known ashes from throughout Iceland. In particular, silicic ashes from Hekla have been well studied [*Larsen and Thórarinsson*, 1978; *Thorarinsson*, 1979] and their ages have been determined from multiple localities [e.g., *Dugmore et al.*, 1995]. Age constraints from tephrochronology involve extrapolation of the section beneath the level of an ash of known age. Distinction among the various Hekla deposits is not unequivocal; however, all designations shown in Figure 5 are consistent with known chemical variations,

**Table 2.** Chemical Analyses of Ash Layers[a]

| | *n* | $SiO_2$ | $TiO_2$ | $Al_2O_3$ | FeO* | MnO | MgO | CaO | $Na_2O$ | $K_2O$ | $P_2O_5$ | Sum |
|---|---|---|---|---|---|---|---|---|---|---|---|---|
| | | | | | | *Kráksh raun* | | | | | | |
| IT-235-j | *5* | 49.88 | 2.99 | 12.73 | 13.87 | 0.21 | 5.45 | 10.00 | 2.61 | 0.42 | 0.30 | 98.47 |
| IT-235-i | *7* | 50.36 | 3.20 | 12.76 | 14.48 | 0.24 | 5.19 | 9.89 | 2.68 | 0.44 | 0.32 | 99.57 |
| IT-235-h | *5* | 50.16 | 3.17 | 12.41 | 14.41 | 0.24 | 5.08 | 9.87 | 2.62 | 0.44 | 0.31 | 98.71 |
| IT-235-f | *5* | 47.73 | 3.50 | 14.41 | 14.40 | 0.23 | 6.09 | 10.50 | 2.63 | 0.46 | 0.36 | 100.32 |
| IT-235-e | *1* | 77.98 | 0.18 | 12.21 | 2.27 | 0.10 | 0.02 | 0.99 | 3.92 | 2.94 | 0.00 | 100.61 |
| | *9* | 51.12 | 1.34 | 15.18 | 11.12 | 0.20 | 8.31 | 12.77 | 2.07 | 0.07 | 0.20 | 102.38 |
| IT-235-d | *7* | 49.90 | 1.25 | 14.95 | 11.24 | 0.20 | 8.01 | 12.80 | 2.17 | 0.07 | 0.12 | 100.72 |
| IT-235-c | *3* | 69.26 | 0.33 | 12.73 | 4.13 | 0.15 | 0.22 | 1.39 | 4.81 | 2.92 | 0.07 | 96.00 |
| | *2* | 63.42 | 1.51 | 12.92 | 8.62 | 0.16 | 1.31 | 4.67 | 3.43 | 1.60 | 0.49 | 98.12 |
| IT-235-b | *7* | 48.07 | 3.22 | 15.01 | 14.49 | 0.23 | 6.08 | 10.30 | 2.85 | 0.42 | 0.30 | 100.97 |
| IT-235-a | *3* | 49.14 | 4.19 | 13.84 | 13.89 | 0.21 | 5.19 | 10.52 | 3.01 | 0.59 | 0.50 | 101.08 |
| | *3* | 50.49 | 2.81 | 14.17 | 13.85 | 0.25 | 5.63 | 10.45 | 2.54 | 0.40 | 0.29 | 100.90 |
| | | | | | | *Kjalhraun* | | | | | | |
| IT-287-f | *3* | 58.44 | 1.57 | 14.38 | 10.35 | 0.29 | 2.30 | 5.88 | 3.48 | 1.39 | 0.76 | 98.84 |
| IT-287-e | *3* | 75.77 | 0.12 | 12.88 | 1.98 | 0.09 | 0.01 | 1.36 | 4.41 | 2.96 | 0.01 | 99.59 |
| IT-287-c | *5* | 48.73 | 4.12 | 12.95 | 14.24 | 0.21 | 4.71 | 9.78 | 3.01 | 0.83 | 0.63 | 99.21 |
| IT-287-b | *4* | 68.56 | 0.34 | 13.99 | 5.63 | 0.18 | 0.33 | 3.09 | 4.37 | 2.20 | 0.12 | 98.81 |
| | *3* | 75.40 | 0.08 | 12.32 | 1.72 | 0.06 | 0.02 | 1.29 | 4.16 | 2.95 | 0.02 | 98.01 |
| IT-287-a | *7* | 49.96 | 1.13 | 14.42 | 10.56 | 0.19 | 7.92 | 13.18 | 2.06 | 0.09 | 0.19 | 99.69 |
| IT-280 | *5* | 51.88 | 3.23 | 12.85 | 14.38 | 0.27 | 5.38 | 10.04 | 2.08 | 0.75 | 0.32 | 101.18 |
| | *1* | 50.80 | 1.41 | 14.49 | 12.42 | 0.23 | 7.43 | 12.55 | 2.05 | 0.12 | 0.10 | 101.58 |
| | *1* | 49.16 | 4.27 | 13.59 | 13.92 | 0.26 | 5.32 | 11.23 | 2.03 | 0.53 | 0.47 | 100.77 |
| | *1* | 54.46 | 2.28 | 15.47 | 10.55 | 0.19 | 4.48 | 10.12 | 3.42 | 0.34 | 0.49 | 101.79 |
| | *1* | 60.35 | 1.60 | 13.39 | 12.64 | 0.33 | 1.43 | 5.67 | 3.23 | 1.57 | 1.33 | 101.55 |
| | | | | | | *Sköflungur* | | | | | | |
| IT-326-f | *5* | 48.52 | 4.71 | 12.32 | 14.47 | 0.25 | 4.93 | 9.96 | 3.07 | 0.70 | 0.68 | 99.61 |
| IT-326-e | *4* | 65.84 | 0.60 | 14.55 | 7.23 | 0.23 | 0.80 | 4.28 | 4.46 | 1.72 | 0.28 | 99.99 |
| | *2* | 49.64 | 2.07 | 14.15 | 11.33 | 0.21 | 7.27 | 12.29 | 2.20 | 0.24 | 0.28 | 99.69 |
| IT-326-d | *9* | 48.90 | 4.52 | 12.83 | 14.74 | 0.23 | 5.01 | 10.27 | 2.94 | 0.68 | 0.52 | 100.64 |
| IT-326-c | *8* | 58.60 | 1.67 | 14.22 | 10.44 | 0.28 | 2.39 | 6.07 | 3.51 | 1.32 | 0.86 | 99.36 |
| | *2* | 75.98 | 0.11 | 12.70 | 2.06 | 0.07 | 0.01 | 1.36 | 4.34 | 2.87 | 0.02 | 99.52 |
| IT-326-b | *3* | 63.06 | 1.09 | 13.91 | 7.83 | 0.28 | 1.21 | 4.20 | 4.30 | 1.80 | 0.55 | 98.24 |
| | *1* | 74.99 | 0.07 | 12.51 | 1.95 | 0.08 | 0.03 | 1.35 | 4.20 | 2.76 | 0.05 | 97.99 |
| IT-326-a | *3* | 50.21 | 1.96 | 14.65 | 11.28 | 0.24 | 7.46 | 12.37 | 2.31 | 0.30 | 0.23 | 101.01 |
| | *2* | 52.11 | 3.91 | 12.99 | 12.86 | 0.26 | 3.90 | 8.44 | 3.60 | 1.16 | 0.63 | 99.86 |
| | *1* | 68.00 | 1.22 | 13.70 | 5.25 | 0.18 | 1.05 | 2.83 | 4.07 | 2.78 | 0.29 | 99.38 |
| | | | | | | *Selvogsheiði* | | | | | | |
| IT-331-i | *4* | 48.30 | 4.89 | 12.42 | 15.16 | 0.24 | 5.06 | 10.06 | 2.88 | 0.77 | 0.54 | 100.29 |
| IT-331-h | *2* | 61.64 | 0.81 | 18.32 | 5.78 | 0.12 | 0.71 | 6.44 | 4.83 | 1.44 | 0.35 | 100.44 |
| | *2* | 66.28 | 0.95 | 14.56 | 5.96 | 0.16 | 0.76 | 3.79 | 4.54 | 2.44 | 0.35 | 99.77 |
| | *2* | 59.75 | 1.40 | 13.29 | 11.21 | 0.32 | 3.44 | 5.91 | 3.61 | 1.35 | 0.69 | 100.96 |
| IT-331-g | *6* | 47.94 | 4.53 | 12.42 | 14.87 | 0.22 | 4.96 | 9.85 | 3.03 | 0.71 | 0.50 | 99.04 |
| IT-331-f | *7* | 47.71 | 4.57 | 12.55 | 14.68 | 0.23 | 5.12 | 10.33 | 2.92 | 0.65 | 0.46 | 99.22 |
| IT-331-e | *2* | 48.44 | 4.51 | 12.56 | 15.25 | 0.22 | 5.09 | 10.60 | 2.84 | 0.64 | 0.45 | 100.60 |
| IT-331-d | *3* | 48.95 | 4.68 | 10.98 | 15.16 | 0.23 | 4.67 | 9.89 | 2.89 | 0.86 | 0.52 | 98.85 |
| | *2* | 67.54 | 1.25 | 13.53 | 5.56 | 0.17 | 1.19 | 3.32 | 4.47 | 2.48 | 0.24 | 99.76 |
| IT-331-c | *3* | 53.91 | 2.94 | 13.25 | 14.45 | 0.23 | 5.54 | 9.93 | 2.73 | 0.35 | 0.32 | 103.66 |
| IT-331-b | *4* | 53.64 | 1.50 | 14.22 | 12.32 | 0.23 | 6.36 | 12.24 | 2.32 | 0.13 | 0.14 | 103.09 |
| IT-331-a | *6* | 52.56 | 1.49 | 13.60 | 11.27 | 0.20 | 7.53 | 13.16 | 2.02 | 0.10 | 0.09 | 102.03 |
| | | | | | | *Strýturhraun* | | | | | | |
| IT-374-f | *7* | 75.86 | 0.11 | 14.63 | 2.10 | 0.08 | 0.04 | 1.32 | | 2.60 | 0.02 | 96.77 |
| IT-374-e | *6* | 47.65 | 4.63 | 14.12 | 15.17 | 0.24 | 5.35 | 10.00 | 2.51 | 0.79 | 0.48 | 100.93 |
| IT-374-d | *6* | 76.22 | 0.08 | 14.17 | 1.88 | 0.07 | 0.06 | 1.25 | | 2.44 | 0.03 | 96.18 |
| | *6* | 69.03 | 0.39 | 16.50 | 6.51 | 0.21 | 0.47 | 3.16 | | 1.98 | 0.11 | 98.35 |
| IT-374-c | *10* | 49.23 | 3.21 | 14.35 | 14.74 | 0.24 | 5.94 | 9.84 | 2.54 | 0.44 | 0.35 | 100.88 |
| IT-374-b | *7* | 49.19 | 3.14 | 14.44 | 14.36 | 0.25 | 6.24 | 10.01 | 2.57 | 0.48 | 0.34 | 101.01 |
| IT-359-a | *5* | 75.18 | 0.31 | 14.26 | 2.67 | 0.10 | 0.25 | 1.54 | 4.17 | 2.56 | 0.05 | 101.09 |

**Table 2.** (continued)

| | *n* | $SiO_2$ | $TiO_2$ | $Al_2O_3$ | FeO* | MnO | MgO | CaO | $Na_2O$ | $K_2O$ | $P_2O_5$ | Sum |
|---|---|---|---|---|---|---|---|---|---|---|---|---|
| | | | | | | *Lambahraun* | | | | | | |
| IT-276-c | *4* | 48.29 | 4.58 | 12.77 | 14.7 | 0.24 | 4.74 | 10.07 | 2.79 | 0.80 | 0.52 | 99.49 |
| IT-276-d | *4* | 47.42 | 3.94 | 12.79 | 13.86 | 0.21 | 5.62 | 11.10 | 2.82 | 0.55 | 0.38 | 98.69 |
| IT-276-e | *6* | 74.40 | 0.13 | 11.89 | 1.56 | 0.04 | 0.07 | 0.70 | 3.70 | 3.73 | 0.03 | 96.25 |

[a] All analyses by electron microprobe at University of Iceland; sample numbers refer to ash horizons shown in Figure 5; *n* denotes number of analyses averaged. All values in wt% FeO* is total Fe expressed as FeO.

**Table 3.** Postglacial Lava Units, Western Volcanic Zone[a]

| | Unit | Age, years B.P. | Area, $km^2$ | | Volume, $km^3$ | Vent Type |
|---|---|---|---|---|---|---|
| | | | Map | Est. | | |
| | | | *Postglacial Lava Units* | | | |
| Svínahraunsbruni | krt | 950 | 12.4 | 12.4 | 0.1 | ‘a‘ā lava from short fissure |
| Hallmundarhraun | hmh | 1050 | 243 | 255* | 8.5 | lava shield |
| Nesjahraun | nsh | 1800 | 30 | 38 | 0.4 | fissure eruption |
| Thjófahraun | tfh | 3600 | 51.5 | 51.5 | 1.0 | fissure eruption |
| Lambahraun | lbh | 4000 | 145 | 145 | 7.3 | lava shield |
| Krákshraun | kkh | (4500) | 36 | 36 | 0.5 | small shield; >H5 |
| Leitahraun/ Ellidaárhraun | lth ell | 5200 | 88 | 104 | 6.3 | lava shield |
| Sköflungur | sfh | (5300) | 44 | 44 | 0.9 | small shield; >H4 |
| Hagafellshraun | hfh | | 3 | 3 | 0.03 | small shield |
| Strýtuhraun | sth | (5500) | 11.5 | 11.5 | 0.2 | small shield; >H4, <H5 |
| Hagavíkurhraun | hvh | 5700 | 21 | 41 | 0.4 | fissure eruption |
| NE Langjökull | nel | | 1 | 20* | 0.2 | unknown source beneath Langjökull |
| Jökulkrókur | jkr | | 0.2 | 10* | 0.1 | unknown source beneath Langjökull |
| Stangarháls | shh | | 0.5 | 2.5 | 0.03 | short fissure |
| Eldborgir | ebh | | 49 | 65 | 1.6 | fissure eruption |
| Kjalhraun | kjh | (7800) | 178 | 182 | 10.9 | lava shield; >H5 |
| Geitlandshraun II | glh | 8900 | 62 | 62 | 1.5 | small shield |
| Skjaldbreiður II | Sk-II | | 135 | 135 | 10.8 | lava shield |
| Skjaldbreiður I | Sk-I | | 35 | 90 | 2.7 | unknown vent structure |
| Gjábakkahraun | gbh | | 25 | 38 | 1.1 | small shield |
| Grímsnes | | ~8200–9700 | | | 0.6 | flank lava field from 10 separate eruptive centers |
| Brunnar/Skógarkot | bsh | | 32 | 62 | 1.2 | small shield (?) |
| Selvogsheiði | svh | (9500) | 24 | 27 | 0.8 | small shield |
| Ásar | dda | | 4.4 | 6 | 0.2 | picritic lava shield |
| Búrfell | bfh | | 2 | 6 | 0.1 | picritic lava shield |
| Hafnarhraun | hnh | | 39 | 105 | 4.2 | shield lava |
| Thingvallahraun | tvh | 10200 | 31 | 135 | 10.8 | shield lava; source unknown |
| Hellisheiði A | hea | 10300 | 7.5 | 34 | 1.2 | shield lava |
| Geitlandshraun I | gl-I | | 0.6 | 5.6 | 0.1 | source beneath Langjökull |
| Tjarnahnúkur | tjh | | 4 | 4 | 0.1 | Strombolian cone and flow |
| | | | *Finiglacial Lava Units* | | | |
| Heiðin há | hhh | | 117 | 164 | 9.8 | lava shield |
| Hagafell shield | hfs | | 14 | 30 | 4.5 | shield lava, source beneath Langjökull |
| N. Langjökull | nlj | | 3.3 | 53* | 5.3 | shield lava, source beneath Langjökull |
| Jökulstallar | jsh | | 31 | 80* | 8.1 | shield lava, source beneath Langjökull |
| Leggjabrjótur | lgh | | 42 | 63 | 6.3 | lava shield |

[a] Absolute ages (calibrated in years before 1950 A.D.) are constrained by $^{14}C$ (Table 1). Ages in parentheses are approximate ages based on relationship to known ash layers (see text); H4, H5 denote the Hekla 4 and Hekla 5 ashes of *Larsen and Thórarinsson* [1978]. Areas are given as both the actual map areas and estimated original areas, where data allow. Estimated areas marked with an asterisk (*) include poorly constrained estimated areas beneath Langjökull. Finiglacial lava units contain evidence for interaction with glacial ice or meltwater.

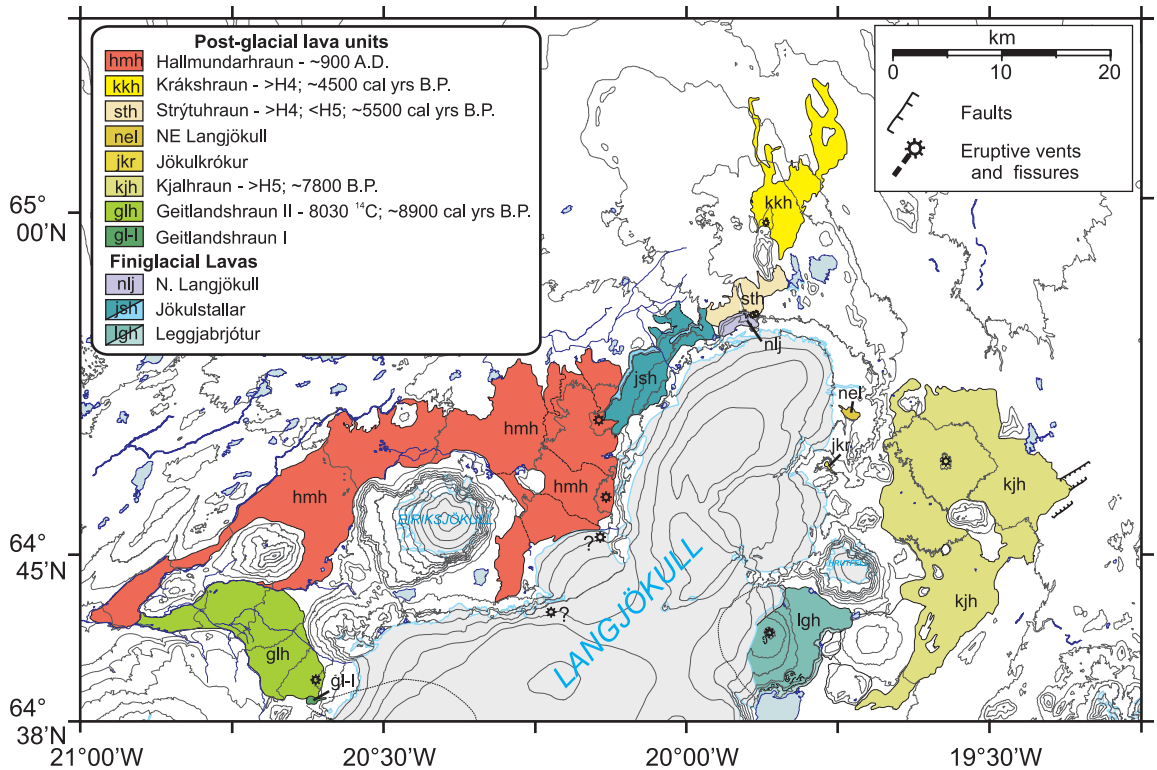


**Figure 6.** Geologic map showing distribution of postglacial lava units in the northern part of the WVZ, modified from *Kjartansson* [1983] and *Jóhannesson and Sæmundsson* [1998]. Contacts extending beneath Langjökull are based on subglacial topographic data (H. Björnsson, personal communication, 2001).

as well as the thicknesses of these ash deposits predicted by the isopach maps of *Larsen and Thórarinsson* [1978]. We have used calibrated ages for the H3, H4 and H5 ashes of 2900, 4200 and 6100 cal years B.P., respectively [*Dugmore et al.*, 1995].

[12] The age of Strýtuhraun is well constrained to be ~5500 B.P because it occurs 40 cm below the Hekla 4 ash, and 15 cm above Hekla 5. We assign an age of ~5300 years to the Sköflungur lava that occurs 19 cm below the ~Hekla 4 ash. Krákshraun lies immediately below Hekla 4, while Hekla 5 overlies Kjalhraun by 22 cm. A provisional age of ~9500 years is assigned to Selvogsheiði by assuming that ash layer *f* (Figure 5) is the 3660 cal. years B.P. Katla (KN) ash. The age of Lambahraun is especially well constrained by the presence of Hekla 3 ash lying ~15 cm below the lava at one of the two sites dated by $^{14}$C (Figure 5; Table 2).

## 4. Eruptive History

[13] We have identified 34 separate eruptive units in the main part of the WVZ, in addition to 10 small units that comprise the Grímsnes field [*Jakobsson*, 1966] (Table 3). In the discussion that follows we have divided the postglacial eruptive history of the WVZ into four general age subdivisions.

### 4.1. Finiglacial Eruptions

[14] Four eruptive units distributed around the present-day glacier Langjökull (jökull = glacier in Icelandic) (Figures 2, 3, and 6) contain evidence for interaction with thin ice sheets or meltwater associated with the latest stages of glaciation. These are the North Langjökull, Jökulstallar and Leggjabrjótur lava shield sequences on the north and east side of Langjökull (Figure 6), and the Hagafell shield to the south (Figure 3). Each of these units has a distinctive morphology, with steep flow fronts up to ~150 m high of pillow lava, pillow breccia and/or hyaloclastite surmounted by gently sloping, large-volume lava shields. Although hyaloclastite is not exposed in the steep front of North Langjökull, subaerial lava that drapes this slope likely buries earlier eruptives of hyaloclastite. Of these four units, the summit crater, Sólkatla, of Leggjabrjótur is the only one for which the eruptive center is not presently

covered by ice. Radiofrequency soundings of the topography beneath Langjökull (H. Björnsson, personal communication, 2001) allow us to extend the contact areas of the Leggjabrjótur and Hagafell shields with confidence (Figure 2).

[15] *Kjartansson* [1964b, 1966b] interpreted the morphology of Leggjabrjótur to reflect early eruptions that interacted with ice or shallow lake waters, followed by subaerial extrusion of shield lava. Two large collapse structures outside the summit crater are thought to represent places where subaerial lava initially flowed over ice, which subsequently melted and allowed the unsupported, solidified lava sheets to collapse into pits ranging up to ~1 km across and 100 m deep. The northern margin of North Langjökull contains a similar large collapse structure, which we interpret to have formed by the same process.

[16] The clear evidence for interaction of these eruptions with small volumes of glacial ice or meltwater argues for a very late glacial to very early postglacial age for these features. The large ratio of subaerial to subaqueous eruptives contrasts with that of Icelandic table mountains or *tuya*, in which a small volume of degassed, subaerial lava surmounts a much higher pedestal of hyaloclastite and pillow lava; the latter are interpreted to represent subglacial eruptions that eventually burned through significant thicknesses of ice or water.

[17] In addition to the above four units, very steep flow fronts along the northeastern boundary of the Heiðin há lava shield in the south (Figure 4), indicates that lava flows from this shield ponded against moderately thick ice in this region. We therefore also tentatively assign a finiglacial age to the Heiðin há lava shield.

## 4.2. Early Postglacial Eruptions

[18] We estimate that another 11 lava shields and at least part of the Grímsnes field formed within the first 3000 years after the ice retreat. $^{14}C$ ages indicate that the Hellisheiði A (Figure 4) and Thingvallahraun (Figure 3) compound lava sequences [*Walker*, 1971] formed 10,300 and 10,200 years B.P., respectively, and we estimate the age of the Hafnarhraun (Figure 4), which *Jónsson* [1978] showed to be younger than Heiðin há, also to have formed about this time (Table 2). Two small picritic lava shields in the southern WVZ (Búrfell and Ásar, Figure 4) are clearly older than the 5200-year-old Leitahraun, but their age is not constrained further. The base of the Búrfell shield is exposed along its SW margin, but at this location it lies directly on interglacial shield lavas (~100,000 years old?) without intervening soil. Although *Jónsson* [1978] suggested that there were three separate shields in the region around Dimmadalsheiði and Ásar (his units D27, D28, D29), chemical data suggest that they represent a single eruptive unit, which we have combined into the Ásar lava shield (Figure 4). We estimate the age of the Selvogsheiði shield (Figure 4) to be about 9,500 years, based on tephrochronology (Figure 5).

[19] In addition to the above six southern shields, two other units were probably erupted about 10,000 years ago. *Sæmundsson* [1995] considered the Tjarnahnúkur eruption (Figure 4) to be early postglacial. The vent for this unit is a large cinder cone, indicating strombolian activity that is otherwise rare in the WVZ. The lava lies directly on gravel and hyaloclastite without intervening soil for much of its length. A sliver of highly phyric lava (gl-I, Figure 6) on the west side of Langjökull is overlain to the north by the 8900-year-old Geitlandshraun II lava and to the east by glacial debris presumably deposited during the little ice age advance of Langjökull. Radiofrequency soundings of the topography beneath Langjökull (H. Björnsson, personal communication, 2001) reveal a nearly conical lava shield lying to the east of this lava outcropping; we tentatively correlate the older Geitlandshraun I lava with this lava shield (Figures 2 and 6).

[20] Skjaldbreiður (Figure 3) is a classic Icelandic lava shield [*Tryggvason*, 1943; *Walker*, 1965; *Guðmundsson et al.*, 2000; *Rossi*, 1996; *Rossi and Sigvaldason*, 1996] with a low-angle pedestal of primarily tube-fed pāhoehoe lavas, surmounted by a steeper cone composed of a mixture of tube-fed and summit-derived surface flows. Although *Rossi* [1996] considered these two parts of Skjaldbreiður to form more or less contemporaneously by different emplacement processes from a common magma system with a total volume of ~15 $km^3$, our work shows that the lower pedestal is almost certainly older than the cone. Furthermore the chemical data indicate that the differences in composition among the three chemical units of the Skjaldbreiður area cannot be related by fractionational crystallization, requiring significant variation in parental magmas arising from mantle melting throughout the evolution of this region. On the basis of geo-

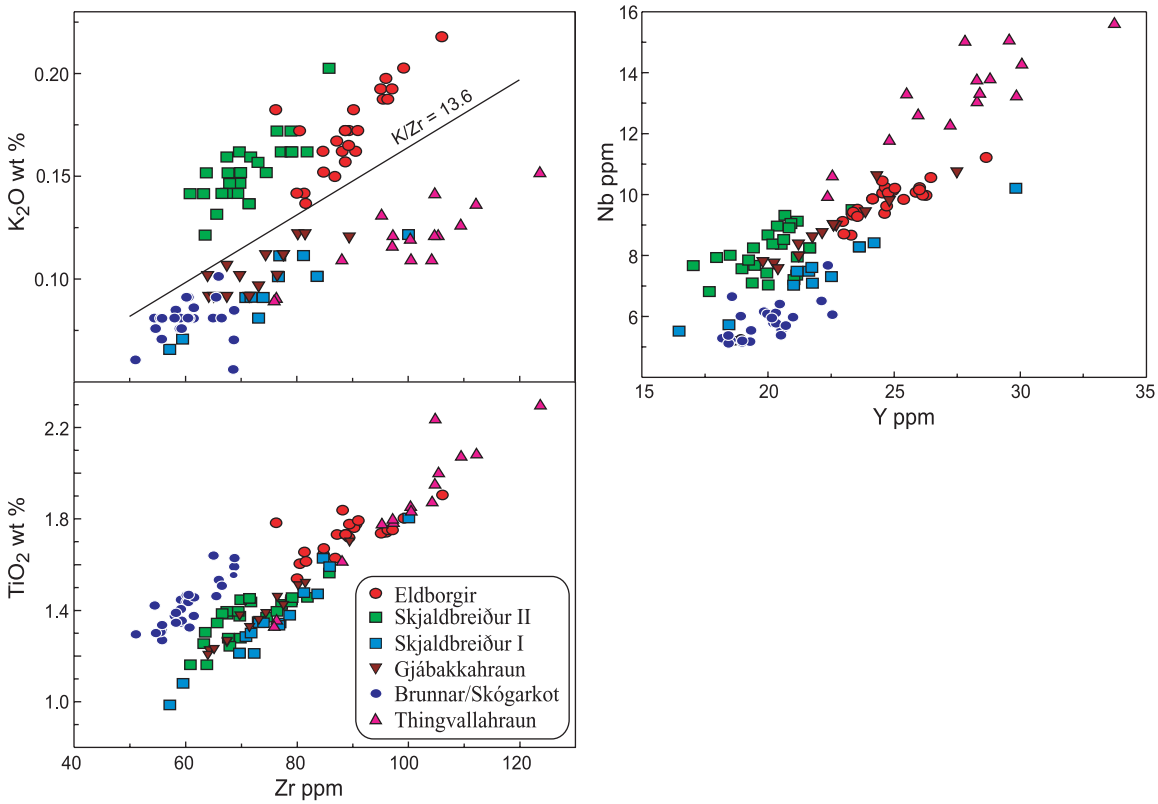


**Figure 7.** Chemical variations (see auxiliary material Table 1) within lava units north of Thingvallavatn. *Sæmundsson* [1992] separated lavas in this region into those from the known eruptive centers at Brunnar, Skaldbreiður, and Eldborgir. On the basis of field relations and geochemical variations such as those shown here, we now recognize six distinct chemical units, for which the geological distribution is shown in Figure 3; the legend shows these units in their correct stratigraphic order. The two youngest units have higher $K_2O$ ($K/Zr > 13.6$) than all older units. The various older units can be distinguished on the basis of field relations coupled to the variations of Ti, Zr, Nb, and Y contents.

logic mapping and rock chemistry we have divided lavas around Skjaldbreiður into three separate eruptive units (Figures 3 and 7). The oldest lavas are low-K, Nb olivine tholeiites with relatively high Ti compared to later lavas from Skjaldbreiður. These lavas (bsh) are found farthest from the present lava shield summit, comprising the Skógarkot lava rise structure [*Walker*, 1991] immediately to the north of Thingvallavatn (Figure 3). Similar composition lavas make up the cones and lava at Brunnar to the west of Skjaldbreiður (Figure 3), which are in turn overlain by lavas with Sk-I compositions. Sk-I lavas have low K and Nb similar to the lavas of Brunnar/Skógarkot (bsh), but also have distinctively lower Ti (Figure 7). They make up the low-angle pedestal of the Skjaldbreiður lava shield; their distribution suggests eruption from vents in the vicinity of the present summit. These lavas are overlain by higher K lavas that make up the main cone of Skjaldbreiður (Sk-II). Sk-II lavas include dense, tube-fed pāhoehoe as well as thin, shelly pāhoehoe flows that overflowed the summit crater.

[21] The relative ages of the bsh, Sk-I and Sk-II units are well constrained by geologic mapping. However, the number of discrete eruptions responsible for this sequence remains in question. Were these three units produced by temporally isolated eruptions, or did magma compositions change during ongoing, sustained eruptive episodes? Contacts between Sk-I and bsh and Sk-II and Sk-I are locally well exposed, and the lack of soil between the lava units at these locations suggests that any eruptive hiatuses must have been very brief. Furthermore, chemical variations within other lava shields of the WVZ, e.g., Lambahraun, Leitahraun, Kjalhraun, require parental magma compositions to have changed during the course of shield development, although the variations are not as extreme as at Skjaldbreiður. Two small cones lying 10 km to the west of the summit of Skjaldbreiður (Figure 3)

are the likely vents for the lava at Brunnar. On the basis of this separation, we consider the Brunnar/Skógarkot lava to be the result of a separate, slightly earlier, eruption than for Skjaldbreiður. The lack of evidence for eruptive breaks within the Skjaldbreiður units identified in this study leads us to consider the Sk-I and Sk-II chemical units to represent evidence for magma evolution during a long, sustained eruptive episode culminating with the development of the Skjaldbreiður lava shield (see section 9.1).

[22] We have subdivided the Elborgir lava of *Sæmundsson* [1992] into four discrete eruptive units (Figure 3) based on new field and geochemical observations. The oldest unit is the early postglacial Thingvallahraun, which is overlain by the lava of Skógarkot (bsh); these two units are discussed above. The Gjábakkahraun lava shield is a newly identified unit that we have traced back to a pair of eruptive vents that lie on a trend of ~N30W, ~1 km south of the Hrafnabjörg table mountain (Figure 3). Gjábakkahraun overlies lavas of Skógarkot, but is older than lavas of Eldborgir and Thjófahraun.

[23] Two new charcoal ages (Table 1) indicate that at least part of the Grímsnes lava field (Figure 2) [*Jakobsson*, 1966] was erupted more than 8000 years B.P. The Grímsnes field is anomalous in many respects compared to other eruptive units of the WVZ. The field is displaced 15–20 km to the SE of the nearest other postglacial WVZ vents (Figure 2) and thus represents a volcanic system that is displaced from the main trend of the WVZ. A swarm of ground fissures trends NE from the volcanic field. The Grímsnes field is volcanically anomalous in being composed of at least 10 eruptive centers, each of which produced relatively small-volume lava flows from well-developed spatter and cinder cones. Finally, the Grímsnes lavas are chemically anomalous, being the most enriched in incompatible elements and having the highest $^{206}Pb/^{204}Pb$ ratios within all of western Iceland [*Chauvel and Hémond*, 2000]. Taken together these data suggest that the Grímsnes field represents a flank field characterized by volumetrically minor lava eruptions, probably derived by low degrees of mantle melting (see section 6).

### 4.3. 9000–6000 Years B.P.

[24] The Geitlandshraun II lava (Figure 6) was erupted from a localized summit cone and crater complex at its eastern end. Thus it represents a small half-shield, with lava covering more than 60 $km^2$. The lava is cut on the south by the Geitá river where it is about 2-m thick, resting on thick soil, river gravels and glaciated Pleistocene shield lava. Charcoal from this region yielded a $^{14}C$ age of 8030 ± 55 years, which calibrates to ~8900 years B.P.

[25] Eldborgir lava (Figure 3) overlies Gjábakkahraun but is partially buried by 3600-year-old Thjófahraun. Much of the faulting that cuts Gjábakkahraun does not continue into the Eldborgir lava, indicating that the latter unit is younger than much of the major faulting associated with the Thingvellir graben. It is notable that the Eldborgir sequence is the oldest, clearly defined fissure eruption in the WVZ, although some of the earlier lavas of Skjaldbreiður may have been fissure fed. The original Eldborgir fissure was at least 15 km long, although this crater row is partially buried by Thjófahraun lava to the north (Figure 3). The oldest Eldborgir lavas with pāhoehoe and transitional lava morphology were erupted from a complex tube system that extended at least 5 km to the south of the most southerly of the row of spatter cones that define the strike of the eruptive fissure. The last phase of the Eldborgir eruption produced ‘a‘ā lava flows that mainly flowed to the southeast.

[26] The 2-km-long crater row of the Stangarháls fissure (Figure 4) is older than the ~5700-year-old Hagavíkurhraun [*Sæmundsson*, 1992, 1995]. On the basis of the soil profile of *Sæmundsson* [1992] we estimate its age to be ~7000–8000 years B.P.

[27] We estimate the age of the large Kjalhraun lava shield on the east side of Langjökull (Figure 6) to be ~7800 years, based on the amount of soil between the lava and the 6100-year-old Hekla 5 ash (Figure 5). Kjalhraun lava lies directly on relatively coarse-grained, black ash up to 15 cm thick in several places. The one location where we analyzed ash grains from below Kjalhraun yielded mixed compositions ranging from olivine tholeiite to more alkalic compositions similar to those from some volcanoes of the eastern volcanic zone (Table 2). Although multiple sources are indicated by the chemical data, the presence of tholeiitic ash might indicate that it is locally derived and that the early phases of the Kjalhraun eruption were at least mildly explosive. Two separate postglacial lava flows, which we refer to as NE Langjökull and Jökulkrókur (Figure 6), occur between the Kjalhraun shield and Langjökull glacier [*Jóhannesson and Sæmundsson*, 1998]. Although clearly postglacial, their absolute ages are unknown. Both were erupted from vents lying farther to the west,

in the region now covered by glacial ice and outwash gravels. The two flows are relatively close in chemical composition; they could represent two separate flow units from a single eruptive episode, possibly a lava shield now buried beneath Langjökull. However, subglacial topography in this region does not reveal a well-defined shield structure, making this interpretation equivocal.

### 4.4. 6000 Years B.P. to Present

[28] The last 11 eruptions of the WVZ are relatively well constrained to have erupted within the last 6000 years. The areal extent, age and mineralogy of Hagavíkurhraun fissure-fed lavas (Figure 4), including those flows locally referred to as Hellisheiðarhraun B/C, are described by *Sæmundsson* [1992, 1995]. New $^{14}$C ages for two sites along the Hengladalsá are consistent with a calibrated age of ~5700 years B.P. as previously determined by *Jónsson* [1977]. The areal extent and age of the Leitin lava shield (Figure 4) also has been well documented by *Sæmundsson* [1995]. Lavas from Leitin overlie older lavas along the Ellidaár (Ellidaárhraun), which *Torfason et al.* [1999] interpret to represent the earliest eruptive phases of the Leitin lava shield. A previous $^{14}$C date of *Hospers* [1953, Table 1] suggested that Ellidaárhraun could be as much as 800 years older than Leitahraun. We have analyzed two new charcoal sites, one not far from the Hliðardalsskóli site of *Kjartansson* [1966a] and one from the Ellidaár valley in Reykjavík. These two sites yield essentially identical ages, confirming the result of *Jónsson* [1971] that Ellidaárhraun is likely to be an early eruptive phase of the monogenetic Leitin lava shield and that the age of this sequence is about 5200 years B.P.

[29] A relatively young lava at Hagafell (Figure 3) [*Jóhannesson and Sæmundsson*, 1998] was erupted from two small spatter cones aligned ~N45E. Much of this lava is transitional to ‘a‘ā, suggesting that this small eruption was probably very short-lived. Although clearly much younger than the finiglacial shield lava on which it occurs, no absolute age constraints exist for this flow. Its youthful appearance suggests an age of ~5000 years or less.

[30] The two most northerly eruptions of the WVZ in postglacial time are the ~4500-year-old Kráksshraun and ~5500-year-old Strýtuhraun (Figure 6); approximate ages for these units are constrained by their relations to Hekla tephras (Figure 5). Both of these are relatively small volume shields; the vent areas are characterized by small spatter cones, rather than summit craters. Lava morphologies in both units are dominantly pāhoehoe to transitional lava, but the latest flow units in Krákshraun are small volume ‘a‘ā, flows that mainly occur in narrow channels. These relations suggest moderately high effusion rates for both units, possibly with lava viscosity increasing in the latest stages of the eruptions.

[31] *Sæmundsson* [1992] described the Sköflungur lava (Figure 3), which forms a small shield of ~1 km$^3$ lying between the larger Skjaldbreiður and Lambahraun shields. Chemical data allow us to refine the position of the contact between Sköflungur and Skjaldbreiður. The presence of Hekla 4 ash 19 cm above Sköflungur lava indicates an age of about 5300 years for this eruption.

[32] Lambahraun (Figure 3), with an age of 4000 years B.P. (Table 1; Figure 5) is one of the youngest lava shields in Iceland. It is a moderately low-elevation, low-angle shield covering >140 km$^2$. Charcoal from two separate sites provide the first radiometric ages for this unit. *Sæmundsson* [1992] identified Thjófahraun (Figure 3) as the youngest lava in the area north of Thingvallavatn, although he considered it to be older than indicated by our new $^{14}$C age (Table 1) and the observation that it was erupted in the interval between two distinct Katla-derived ash layers, which we interpret to be the KE and KN ashes of *Hardardóttir et al.* [2001]. About 1 km$^3$ of lava was erupted from at least 10 separate spatter cones aligned ~N42E over a distance of ~8 km. The oldest parts of this eruption are pāhoehoe, but the youngest flow units are small-volume, plagioclase-phyric ‘a‘ā lavas.

[33] *Sæmundsson* [1992, 1995] documented the age, character and extent of the Nesjahraun eruption (Figure 4). About 0.5 km$^3$ of very uniform lava was erupted from two 10-km-long fissures aligned N30E, one to the north and one to the south of the center of the Hengill central volcano (Figure 4). There is a 9-km-long gap in erupted lava between the two eruptive fissures; this gap corresponds to the central part of Hengill. Nesjahraun fissures nearly coincide with those of Hagavíkurhraun, the last eruption prior to Nesjahraun in the area. The five samples analyzed from Nesjahraun show the least internal chemical variability (7.75 ± 0.05 wt% MgO) of any postglacial lava within the WVZ.

[34] About 800 years later, the large, 900 A.D. Hallmundarhraun eruption was fed from vents

lying close to the northwest margin of Langjökull glacier (Figure 6). Much of the presently exposed field was apparently produced from two craters ~7 km apart near the western margin of northern Langjökull (Figure 6). A third vent lying 3–4 km farther to the SW beneath Langjökull is required to explain a topographic rise and northwesterly flow directions [*Piper*, 1973] in this area, and a fourth vent lying another 8 km to the SW is indicated by topographic considerations and north-facing flow fronts evident in aerial photographs in the southern part of the flow field. On the basis of similar appearance in aerial photographs we currently include the products of all four of these possible vents into the Hallmundarhraun flow field, although the two southernmost units have not yet been sampled. There is therefore some uncertainty in the number of eruptions responsible for the complete flow field. Our interpretation of lava outcrop patterns (Figure 6) suggests that most of the flow field apparently was erupted from the more southerly of the two subaerially exposed vents.

[35] The age of at least part of Hallmundarhraun is known from both carbon dating [*Sæmundsson*, 1966] and tephrostratigraphy [*Jóhannesson*, 1989]. These age determinations were determined on lava that we interpret to have been derived from the more southerly of the two exposed craters, and might not apply to the whole of Hallmundarhraun. Lava samples from the two northern vents are chemically indistinguishable supporting the interpretation that at least this part of the field was co-eruptive. The northern crater is virtually devoid of tephra; it is a collapsed inflationary structure dominated by tilted pāhoehoe slabs dipping outward at ~70 degrees. Although almost the entire flow field of Hallmundarhraun is dense pāhoehoe containing many large lava tubes, several small ‘a‘ā lava flows issued from the northern crater toward the end of this eruption.

[36] One hundred years later, the last known eruption of the WVZ occurred along a 3-km-long, discontinuous fissure close to the summit of the 5200 years B.P. Leitin lava shield (Figure 4). The Svínahraunsbruni eruption [*Jónsson*, 1979], also known as the Christianity lava flow because the eruption occurred while the Icelandic parliament of 1000 A.D. was discussing whether or not to formally accept Christianity as a national religion, produced only about 0.1 $km^3$ of olivine-phyric ‘a‘ā lava from three spatter cones aligned along a N35E trend.

[37] Although the last eruption of the WVZ occurred about 1000 A.D., *Sæmundsson* [1990, 1992] documented a major tectonic rifting event that occurred around 1789 A.D, and possibly an earlier event in the 14th century. The 1789 event did not produce a lava outbreak, but the nature of the earthquake activity, fault displacements and associated subsidence are consistent with emplacement of a dike during a major rifting event affecting much of the Hengill area (Figure 3).

## 5. Structural Lineaments of the WVZ

[38] The volcanic elements of the WVZ include eruptive fissures and lava shields (Figure 8). Between 64°10′N and 64°20′N the distribution of recent eruptive vents is confined to a zone ~6 km in cross-axis width. To the south, the WVZ widens slightly as it merges with the volcanic segments of the Reykjanes Peninsula. To the north, the WVZ widens dramatically so that it is ~25 km wide north of 64°45′N. The overall trend of the WVZ gradually changes from ~025° in the south to 040° near 64°30′N.

[39] In several places the distribution of glacial and postglacial fissure eruptions can be grouped into well-defined segments (e.g., the segment comprising the Eldborgir, Thjófahraun, Skjaldbreiður, and Sköflungur centers of Figure 3). Another well-defined lineament is the Hengill system [*Einarsson and Sæmundsson*, 1987] which passes through the Hengill central volcano (Figure 8) and extends southward as noneruptive ground fissures to include the early postglacial Ásar, Búrfell, and Selvogsheiði lava shields (Figures 4 and 8). Elsewhere the distribution of vents appears to be more diffuse. North of 64°45′N, where the WVZ overlaps with the Hofsjökull Zone (Figure 1), the distribution of many vents beneath Langjökull glacier is unknown and eruptive centers on the northwest side of Langjökull occur in a diffuse cluster. There are short, north-trending alignments on the northwest and northern sides of Langjökull, and NE-trending faults east of Kjalhraun.

[40] The general alignments of volcanic centers south of 64°45′S suggest that eruptions along that part of the plate boundary tend to be localized along a series of overlapping segments. The general coherence of postglacial and earlier subglacial alignments suggests that these segments are relatively long-lived, persisting on timescales lasting at least several tens of thousands of years. Farther to the north, where the WVZ overlaps

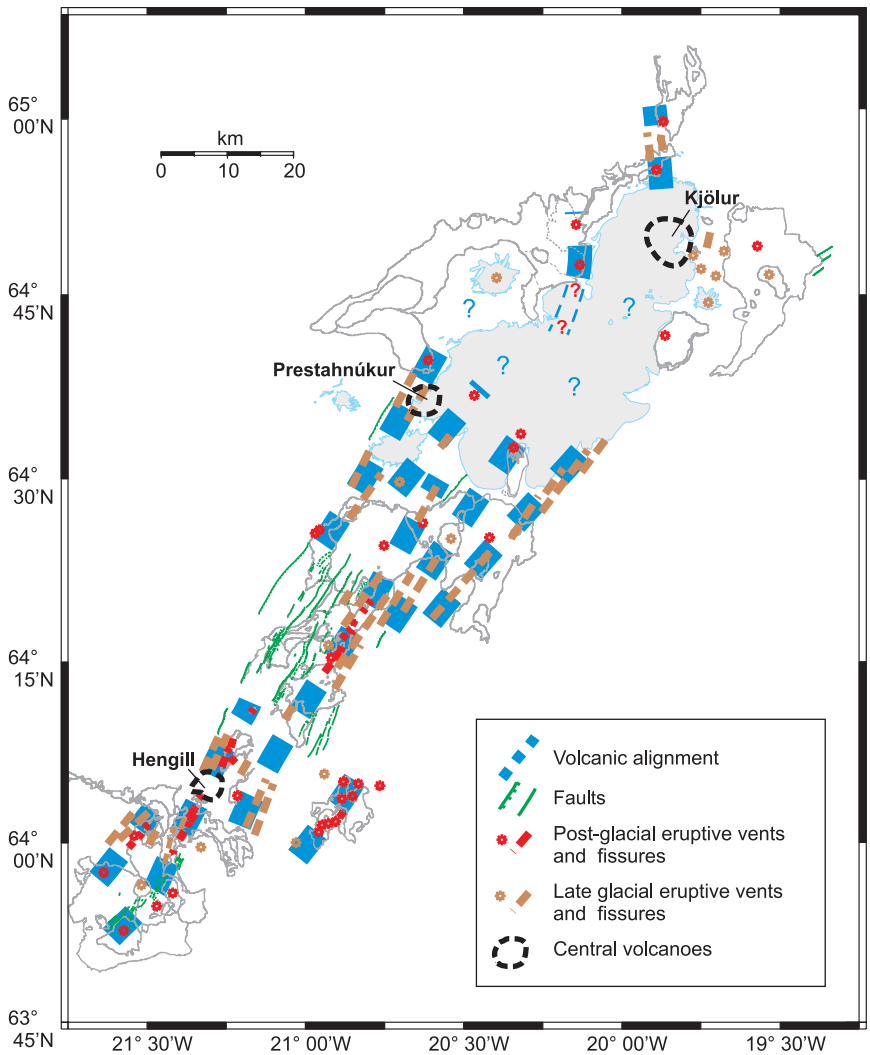


**Figure 8.** Distribution of eruptive vents and principal faults of the WVZ. Late glacial eruptive fissures and vents are mainly defined by hyaloclastite ridges and table mountains, respectively. The locations of the Hengill, Prestahnúkur, and Kjölur central volcanoes [after *Thordarson and Hoskuldsson*, 2002] are shown by heavy dashed lines. The overall structure of the southern WVZ can be described in terms of strongly overlapping volcanic segments. The general coherence of postglacial and earlier subglacial alignments suggests that these segments are relatively long-lived, persisting on timescales lasting at least several tens of thousands of years. Farther to the north, where the WVZ overlaps significantly with the Hofsjökull Zone (Figure 1), any preferred structures are much less evident, owing to significant glacial cover and a tendency for more diffuse distribution of central vents. The southern extension of the lineament on the west side of northern Langjökull (thin dashed lines) is required to explain lava flow directions in the Hallmundarhraun unit (Figure 6), although the exact location of vents beneath Langjökull is not precisely known.

significantly with the Hofsjökull Zone, the lack of evidence for strongly preferred alignments of volcanic centers suggests a more complicated stress regime, possibly evolving over much shorter timescales.

[41] One of the most striking structural features of the WVZ is the well-developed tectonic depression in the Thingvellir area; this depression is now partially filled by lake waters of Thingvallavatn (Figure 3). In this area the inner depression is a highly asymmetric graben [*Sæmundsson*, 1992] with the deepest part immediately to the east of east-facing faults along the western margin. These east-facing scarps (Almannagjá and associated faults) cut postglacial Thingvallahraun and the lava of Skógarkot (Figure 3), and are up to 30–40 m high (Figure 9). *Sæmundsson* [1992] noted that faults cutting older units have greater throws, up to 400 m in units several hundred thousand years old,

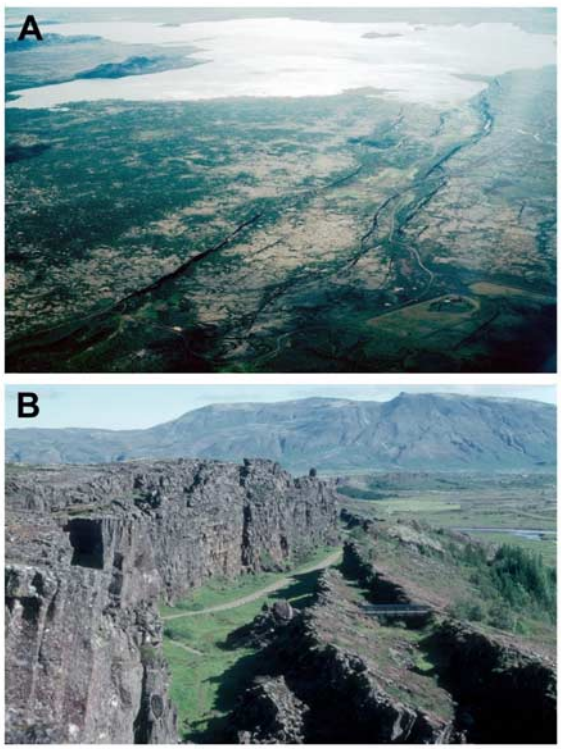


**Figure 9.** Photographs of bounding faults in the Thingvellir area. (top) Oblique aerial photo looking south. The major-east-facing scarp is Allmanagjá. (bottom) View to the north from the top of Allmanagjá, which is about 30 m high. East sloping, slumped lavas on the right are Brunnar/Skógarkot lavas. Lavas at the base of the fault scarp are Thingvallahraun.

which is evidence for the incremental development of the Thingvellir tectonic depression over this period.

[42] South of Thingvallavatn the eruptive fissures associated with the Hengill central volcano (Figure 8) coincide with the axis of the Thingvellir tectonic depression. However, to the west and north of Thingvallavatn the dominant volcanic segment is defined by the Eldborgir and Thjófahraun fissure swarms that cut the eastern flank of the graben, ~8 km to east of the depression axis [*Sæmundsson*, 1992].

[43] Graben structures are a characteristic of several parts of Icelandic rift zones [e.g., *Jakobsson et al.*, 1978; *Björnsson*, 1985; *Gudmundsson*, 1987a, 1987b; *Gudmundsson and Bäckström*, 1991], but the Thingvellir graben is by far the deepest, and characterized by boundary faults with the greatest throws, primarily because this area has not been significantly resurfaced by younger flows since early postglacial time. To the NE of Lake Thingvallavatn, Almannagjá dies out as an east-throwing fault and is replaced by a swarm of west-facing faults centered on Prestahnúkur (Figure 8). In contrast to most Icelandic rift zones which are resurfaced by frequent lava eruptions, near Thingvellir the volcanic axis is displaced more than 8 km to the east and recent lava has only rarely reached the tectonic depression axis. Thus the pronounced subsidence of the Thingvellir depression primarily reflects activity along the Hengill volcanic system, as is manifest by the subsidence and rifting episode of 1789 A.D. [*Sæmundsson*, 1995]. Overall the Thingvellir tectonic depression does not represent a regional low in the volcanic budget along the WVZ, but rather an offset zone between equally productive segments.

[44] Our geologic mapping provides some new constraints on the age and development of the Thingvellir graben in postglacial time. Both Thingvallahraun and lavas of Brunnar/Skógakot (Figure 3) are cut by the major 30–40 m, east-facing scarp of Almannagjá. Lavas of Gjábakkahraun clearly flowed down to the west, indicating topography broadly similar to the present. These lavas are cut by several major, west-facing scarps with little evidence for lava draping earlier structures. In contrast, the lavas of Eldborgir and Thjófahraun show much reduced tectonism and they clearly drape the earlier west-facing scarps, which apparently have not been significantly re-activated since. Thus most of the postglacial tectonism that produced the inner graben in the Thingvellir depression may have occurred in the interval from about 9500–8000 years B.P., i.e., after Skógarkot but prior to Eldborgir.

## 6. Chemical Variations

[45] All postglacial lavas of the WVZ are olivine-normative, tholeiitic basalts. No alkalic or high-silica lavas have been erupted in the WVZ in postglacial time. Even the most alkali-rich lavas from Grímsnes are hypersthene normative and subalkalic. Compared to typical N-MORB, e.g., from the southern East Pacific Rise (EPR) or average N-MORB (Table 4), WVZ basalts are significantly less differentiated with an average MgO of 8.7 wt%. In addition, the average WVZ lava composition is ~1.5–1.6 × higher in Sr, 1.8–2.3 × higher in Rb, 1.4–2.7 × higher in Ba, 2.4–2.8 × higher in Nb, and 40–50% lower in Y than average N-MORB of *Hofmann* [1988] or those from the southern EPR (Table 4), the latter analyzed by the same instrument and methods as for this study. Enrichments in the incompatible

**Table 4 (Representative Sample).** Chemical Analyses of Representative Rock Samples[a] [The full Table 4 is available in the HTML version of this article at http://www.g-cubed.org]

| Sample | IT-318 | IT-261 | IT-187 | IT-42B | IT-183 | IT-231 | IT-192 | IT-25 | IT-454 | IT-359B | IT-19 | IT-238 | IT-408 | IT-101 | IT-58 | IT-242 | IT-250 | IT-178 | IT-32 | IT-87 | IT-223 | IT-328 | IT-305 |
|---|---|---|---|---|---|---|---|---|---|---|---|---|---|---|---|---|---|---|---|---|---|---|---|
| Unit[b] | krt | hmh | nsh | tfh | lbh | kkh | lth | sfh | hfh | sth | hvh | nel | jkr | shh | ebh | kjh | glh | Sk-II | Sk-I | gbh | bsh | svh | dda |
| $SiO_2$ | 47.93 | 47.87 | 48.76 | 48.47 | 48.57 | 47.97 | 48.56 | 48.21 | 47.95 | 48.32 | 48.66 | 48.61 | 48.99 | 48.50 | 47.68 | 48.03 | 47.75 | 48.23 | 47.58 | 48.45 | 48.03 | 49.47 | 47.84 |
| $TiO_2$ | 1.75 | 1.54 | 1.63 | 1.81 | 1.71 | 1.31 | 1.71 | 1.76 | 1.81 | 1.23 | 1.52 | 1.15 | 1.16 | 1.33 | 1.73 | 1.38 | 1.64 | 1.44 | 1.29 | 1.36 | 1.46 | 1.31 | 0.54 |
| $Al_2O_3$ | 14.99 | 15.30 | 14.67 | 14.84 | 15.88 | 16.12 | 15.17 | 15.46 | 15.04 | 15.95 | 14.87 | 15.89 | 15.73 | 15.42 | 15.14 | 16.12 | 14.63 | 15.60 | 16.35 | 15.62 | 15.45 | 14.60 | 15.82 |
| FeO* | 11.84 | 11.58 | 12.43 | 12.56 | 11.59 | 11.19 | 12.05 | 11.83 | 14.19 | 11.82 | 12.06 | 11.45 | 11.04 | 11.11 | 12.26 | 10.77 | 12.74 | 11.00 | 10.92 | 11.11 | 11.34 | 10.97 | 8.62 |
| MnO | 0.22 | 0.21 | 0.20 | 0.20 | 0.18 | 0.19 | 0.19 | 0.19 | 0.19 | 0.18 | 0.20 | 0.16 | 0.14 | 0.19 | 0.20 | 0.17 | 0.15 | 0.18 | 0.17 | 0.18 | 0.19 | 0.16 | 0.19 |
| MgO | 8.74 | 9.54 | 7.71 | 8.05 | 7.75 | 8.96 | 8.40 | 8.05 | 7.57 | 8.59 | 7.93 | 8.94 | 8.85 | 8.08 | 8.99 | 9.34 | 9.71 | 8.53 | 9.49 | 8.66 | 9.71 | 8.51 | 12.19 |
| CaO | 11.99 | 11.56 | 12.30 | 11.73 | 12.52 | 12.38 | 12.10 | 12.17 | 11.55 | 11.88 | 12.52 | 12.50 | 12.68 | 13.03 | 11.64 | 12.47 | 11.63 | 12.56 | 12.14 | 12.90 | 12.20 | 13.88 | 13.10 |
| $Na_2O$ | 2.05 | 2.05 | 1.63 | 1.95 | 1.42 | 1.71 | 1.47 | 1.88 | 1.72 | 1.82 | 1.94 | 1.56 | 1.63 | 1.47 | 1.91 | 1.93 | 1.63 | 1.65 | 1.66 | 1.81 | 1.91 | 1.80 | 1.42 |
| $K_2O$ | 0.21 | 0.16 | 0.18 | 0.21 | 0.13 | 0.07 | 0.15 | 0.16 | 0.18 | 0.10 | 0.16 | 0.06 | 0.08 | 0.12 | 0.16 | 0.08 | 0.11 | 0.17 | 0.09 | 0.10 | 0.09 | 0.05 | 0.01 |
| $P_2O_5$ | 0.17 | 0.16 | 0.15 | 0.19 | 0.21 | 0.10 | 0.16 | 0.18 | 0.15 | 0.07 | 0.13 | 0.06 | 0.08 | 0.11 | 0.16 | 0.08 | 0.12 | 0.14 | 0.13 | 0.16 | 0.12 | 0.07 | 0.02 |
| Sum | 99.88 | 99.99 | 99.67 | 100.01 | 99.97 | 99.99 | 99.96 | 99.91 | 100.35 | 99.96 | 99.98 | 100.40 | 100.39 | 99.35 | 99.85 | 100.37 | 100.12 | 99.50 | 99.81 | 100.33 | 100.50 | 100.82 | 99.75 |
| Sc | 39 | 39 | 44 | 41 | 39 | 39 | 39 | 40 | 42 | 40 | 45 | 41 | 39 | 41 | 40 | 39 | 41 | 39 | 38 | 41 | 38 | 46 | 41 |
| V | 331 | 315 | 346 | 343 | 296 | 302 | 322 | 345 | 340 | 306 | 351 | 279 | 275 | 319 | 325 | 278 | 331 | 302 | 263 | 292 | 275 | 347 | 225 |
| Cr | 390 | 464 | 146 | 304 | 306 | 228 | 317 | 321 | 159 | 76 | 172 | 211 | 207 | 175 | 386 | 370 | 424 | 279 | 369 | 330 | 446 | 443 | 793 |
| Co | 50 | 56 | 54 | 53 | 48 | 55 | 53 | 53 | 50 | 58 | 55 | 55 | 51 | 51 | 56 | 56 | 57 | 51 | 55 | 53 | 55 | 45 | 56 |
| Ni | 133 | 191 | 82 | 112 | 91 | 155 | 125 | 129 | 96 | 137 | 88 | 151 | 139 | 95 | 152 | 176 | 191 | 109 | 162 | 119 | 192 | 102 | 302 |
| Cu | 145 | 98 | 158 | 155 | 161 | 151 | 132 | 140 | | | 166 | | | 132 | 136 | | | 145 | 129 | 130 | 130 | 128 | 111 |
| Zn | 89 | 92 | 94 | 101 | 84 | 86 | 93 | 93 | 98 | 89 | 92 | 81 | 73 | 81 | 96 | 78 | 100 | 83 | 83 | 82 | 82 | 73 | 54 |
| Rb | 3.9 | 2.9 | 3.5 | 3.3 | 2.3 | 1.6 | 2.7 | 2.5 | 4.7 | 2.5 | 3.0 | 1.1 | 2.0 | 2.1 | 2.1 | 1.5 | 2.6 | 2.9 | 0.9 | 1.7 | 1.4 | 1.1 | 0.6 |
| Sr | 198 | 170 | 187 | 191 | 201 | 145 | 176 | 184 | 186 | 120 | 184 | 119 | 127 | 174 | 178 | 190 | 169 | 183 | 160 | 166 | 156 | 129 | 62 |
| Y | 24 | 23 | 24 | 27 | 25 | 20 | 25 | 25 | 26 | 22 | 23 | 20 | 20 | 19 | 25 | 19 | 22 | 21 | 21 | 23 | 21 | 19 | 15 |
| Zr | 91 | 87 | 82 | 111 | 95 | 55 | 88 | 91 | 79 | 53 | 74 | 47 | 52 | 61 | 89 | 50 | 69 | 79 | 71 | 73 | 66 | 36 | 19 |
| Nb | 11.5 | 10.1 | 9.3 | 12.7 | 11.3 | 5.0 | 9.7 | 10.4 | 10.0 | 4.6 | 8.2 | 4.3 | 4.8 | 6.5 | 10.1 | 4.3 | 8.2 | 9.1 | 7.5 | 9.0 | 5.7 | 3.1 | 1.0 |
| Ba | 20 | <12 | 34 | 46 | 43 | <12 | 34 | 38 | 45 | <11 | 26 | <10 | <10 | 30 | 40 | <11 | 27 | 40 | 10 | 17 | 18 | <11 | <11 |

[a] All analyses on whole rock powders by X-ray fluorescence at University of Hawai'i.
[b] Unit designations are those of Table 3. Grímsnes samples IT-288 and IT-289 are from Álftarhóll and Tjarnarhólar, respectively. FeO* = total Fe as FeO.
[c] WVZ ave = average of 309 analyses from throughout the WVZ (excluding analyses of samples from the Grímsnes volcanic field).
[d] Average of 118 analyses of whole rock N-MORB from the southern East Pacific Rise, 13°–23°S [*Sinton et al.*, 1991; *Mahoney et al.*, 1994; J. M. Sinton, unpublished data] analyzed by the same instrument and methods as for this study.
[e] Average N-MORB of *Hofmann* [1988].

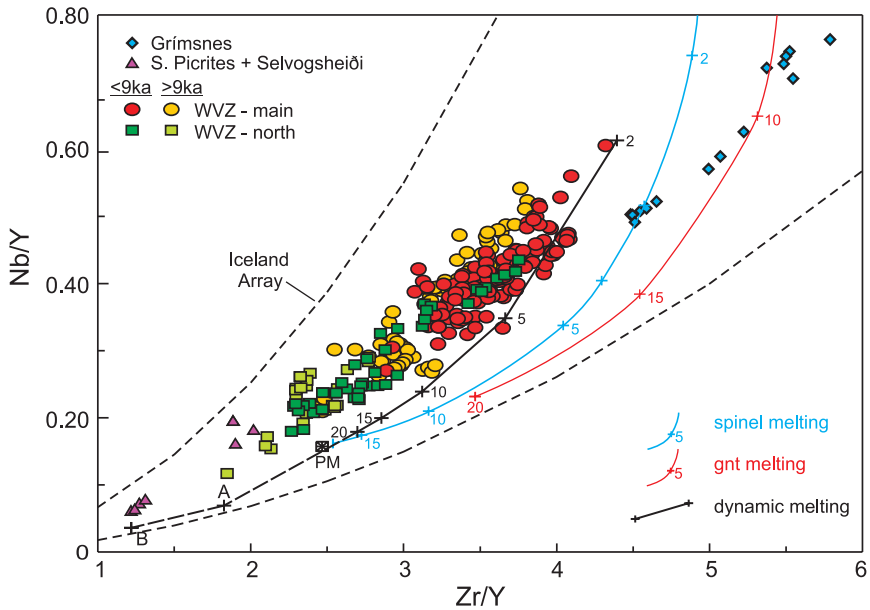


**Figure 10.** Nb/Y versus Zr/Y for all lavas analyzed in this study (see auxiliary material Table 1). Dashed lines bound the Iceland array of *Fitton et al.* [1997]. Samples from lava units of Figure 6 are shown as squares; other WVZ lavas are circles, except as noted in the legend. Lavas older than 9000 years B.P. have a lighter color shading than younger lavas within the main and northern groups. In general, lavas from the northern WVZ have lower Nb/Y and Zr/Y than lavas farther south. See text for discussion. Simplified nonmodal, accumulated fractional melting trends were calculated for melting of spinel- and garnet-peridotite with 0.713 ppm Nb, 11.2 ppm Zr, and 4.55 ppm Y using mineral modes and melt proportions from *Johnson et al.* [1990], and mineral-melt partition coefficients for Nb, Zr, and Y, respectively, of 0.00005, 0.00068, 0.0098 (olivine), 0.0023, 0.01, 0.0538 (opx), 0.0075, 0.1887, 0.3777 (cpx), 0.0384, 1.51, 4.11 (garnet), and 0.08, 0.06, 0.0001 (spinel). Primitive mantle compositions of *Sun and McDonough* [1989] and *Hofmann* [1988] plot within box designated PM. The dynamic melting trend was calculated with 2% melting in the garnet field, followed by 2, 5, 10, 15, and 20% melting in the spinel field. The dashed part of the dynamic melting curve shows melts produced from continued melting of residues from earlier steps. Pt. A is a 5% melt of the residue after the 2% melting described above; pt. B is a 5% melt from the residue after melting that yielded pt. A. All dynamic melting calculations assume 1% retained melt.

elements Rb, Ba, Nb and Sr in ocean island magmas are generally considered to reflect melting of mantle sources that are enriched in these elements relative to depleted MORB mantle. Lower Y values most likely indicate significant melting within the garnet-peridotite stability field. The chemical characteristics of WVZ magmas are generally typical of those associated with hot spot-affected ridges [*Schilling*, 1973a, 1973b; *Schilling et al.*, 1983].

[46] With respect to Nb-Zr-Y variations, all WVZ lavas plot within the Iceland array of *Fitton et al.* [1997] (Figure 10). These elements are all analyzed accurately by XRF methods at their levels of abundance in these samples (Table 5). *Fitton et al.* [1997, 2003], showed that moderately high Nb/Y and Zr/Y, compared to typical N-MORB, is a general feature of Icelandic basalts, which they attributed to melting of a moderately enriched, plume-affected mantle with at least some melting occurring within the stability range of garnet. They also showed that the general variations in this diagram can be related to extent of mantle melting (Figure 10), although the general slope of the array and specifically the very low concentrations of incompatible elements in the most depleted basalts is best explained by a dynamic melting process [*Langmuir et al.*, 1977; *Elliot et al.*, 1991; *Devey et al.*, 1994], allowing for retention of some fraction of trapped melt and/or incomplete mixing of melts from different parts of the upwelling mantle column.

[47] It is well known that mantle being melted beneath Iceland is isotopically, and presumably chemically heterogeneous [e.g., *O'Nions et al.*, 1976; *Hémond et al.*, 1993; *Hanan and Schilling*, 1997; *Chauvel and Hémond*, 2000; *Kempton et al.*, 2000; *Fitton et al.*, 2003; *Thirlwall et al.*, 2004]. Nevertheless, comparisons to simple models invoking a single parent can reveal useful

**Table 5.** Chemical Analyses of Rock Standards[a]

| | W-1 | | | BHVO-1 | | | BIR-1 | | |
|---|---|---|---|---|---|---|---|---|---|
| | Accepted | UH | σ | Accepted | UH | σ | Accepted | UH | σ |
| $SiO_2$ | 52.33 | 52.44 | 0.11 | 49.59 | 49.58 | 0.03 | 47.42 | 47.71 | 0.26 |
| $TiO_2$ | 1.07 | 1.10 | 0.02 | 2.69 | 2.73 | 0.00 | 0.95 | 0.98 | 0.01 |
| $Al_2O_3$ | 14.96 | 15.05 | 0.14 | 13.70 | 13.21 | 0.04 | 15.24 | 15.67 | 0.08 |
| $Fe_2O_3$* | 11.25 | 11.30 | 0.05 | 12.39 | 12.55 | 0.05 | 11.31 | 11.68 | 0.12 |
| MnO | 0.17 | 0.16 | 0.01 | 0.17 | 0.14 | 0.01 | 0.17 | 0.17 | 0.00 |
| MgO | 6.60 | 6.63 | 0.03 | 7.22 | 7.26 | 0.04 | 9.61 | 9.64 | 0.04 |
| CaO | 10.97 | 11.00 | 0.06 | 11.32 | 11.51 | 0.08 | 13.14 | 13.30 | 0.05 |
| $Na_2O$ | 2.15 | 2.13 | 0.11 | 2.24 | 2.33 | 0.01 | 1.74 | 1.54 | 0.03 |
| $K_2O$ | 0.64 | 0.64 | 0.01 | 0.52 | 0.53 | 0.01 | 0.03 | 0.01 | 0.00 |
| $P_2O_5$ | 0.13 | 0.13 | 0.01 | 0.27 | 0.27 | 0.00 | 0.05 | 0.02 | 0.01 |
| Sum | 100.27 | 100.57 | | 100.11 | 100.08 | | 99.66 | 100.72 | |
| *n* | | *12* | | | *2* | | | *8* | |
| Sc | 35 | 36 | 1 | 31.8 | 31 | 1 | 44 | 41 | 1 |
| V | 257 | 260 | 7 | 317 | 309 | 7 | 313 | 307 | 2 |
| Cr | 119 | 128 | 1 | 289 | 301 | 3 | 382 | 407 | 2 |
| Co | 47 | 46 | 1 | 45 | 44 | 0.3 | 51 | 54 | 2 |
| Ni | 75 | 77 | 2 | 121 | 126 | 1 | 166 | 169 | 3 |
| Zn | 84 | 86 | 1 | 105 | 104 | 1 | 71 | 68 | 1 |
| Rb | 21.4 | 22.5 | 0.3 | 9.5 | 9.7 | 0.2 | 0.3 | 0.6 | 0.1 |
| Sr | 186 | 189 | 1 | 390 | 394 | 4 | 108 | 111 | 1 |
| Y | 22 | 22 | 0.1 | 27.6 | 26 | 0.2 | 16 | 16 | 0.2 |
| Zr | 95 | 94 | 0.3 | 179 | 175 | 1.6 | 16 | 15 | 0.2 |
| Nb | 7 | 7.5 | 0.3 | 19 | 18.8 | 0.5 | 0.6 | 0.8 | 0.1 |
| Ba | 162 | 155 | 4 | 139 | 124 | 8 | 7 | <14 | |
| *n* | | *6* | | | *5* | | | *5* | |

[a] Chemical analyses of international rock standards by X-ray fluorescence spectrometry at University of Hawai'i obtained along with the data presented in Table 4. Accepted values are those of *Govindaraju* [1994]. $Fe_2O_3$* is total Fe expressed as $Fe_2O_3$. UH data are given as averages of *n* sample analyses with 1σ variation.

information concerning melting processes beneath Iceland [e.g., *Fitton et al.*, 1997]. Although details of the melting processes affecting WVZ magmas are beyond the scope of the present paper, several relatively simplified melting trajectories are shown on Figure 10. It is apparent from these melting trajectories that accumulation of fractional melts from garnet or spinel peridotites with bulk composition similar to primitive mantle (PM) cannot reproduce the Iceland array. *Fitton et al.* [1997] argued that mantle giving rise to Icelandic basalts might be selectively enriched in Nb relative to PM. However, mixing of melts from the dynamic melting trajectory of Figure 10 can account for much of the spread of WVZ lavas, excluding those from the Grímsnes field, for a bulk mantle composition approximating that of primitive mantle. This result is certainly not unique and isotopic evidence indicates that mantle giving rise to Icelandic lavas is notably heterogeneous, including significant contributions from incompatible element depleted components [e.g., *Thirlwall*, 1995; *Kempton et al.*, 2000].

[48] WVZ lava compositions are restricted to Zr/Y values < 6, in contrast to the entire Iceland array of *Fitton et al.* [1997, 2003] which extends to values of Zr/Y = 10. Lavas of the Grímsnes flank zone are displaced from the rest of the WVZ on this diagram, and have the highest Zr/Y of any WVZ lavas. Picritic samples from southern shields have the lowest Zr/Y and Nb/Y similar to high-Mg lavas elsewhere in Iceland [*Fitton et al.*, 2003].

[49] Samples from north of 64°38′N, i.e., those lava units shown on Figure 6, tend to have lower Zr/Y and Nb/Y than those farther south, with the exception of the most southerly picritic shields and Selvogsheiði. In a study of samples extending off axis to Plio/Pleistocene sections, *Schilling et al.* [1982] showed a general decrease in mantle-normalized La/Sm to the north along the WVZ, and *Jakobsson et al.* [2000] showed a general decrease in total alkali elements at constant MgO for subglacial volcanics to the north along the WVZ. Thus all available evidence indicates a decrease in incompatible element concentrations in the most northerly units. Although it might be

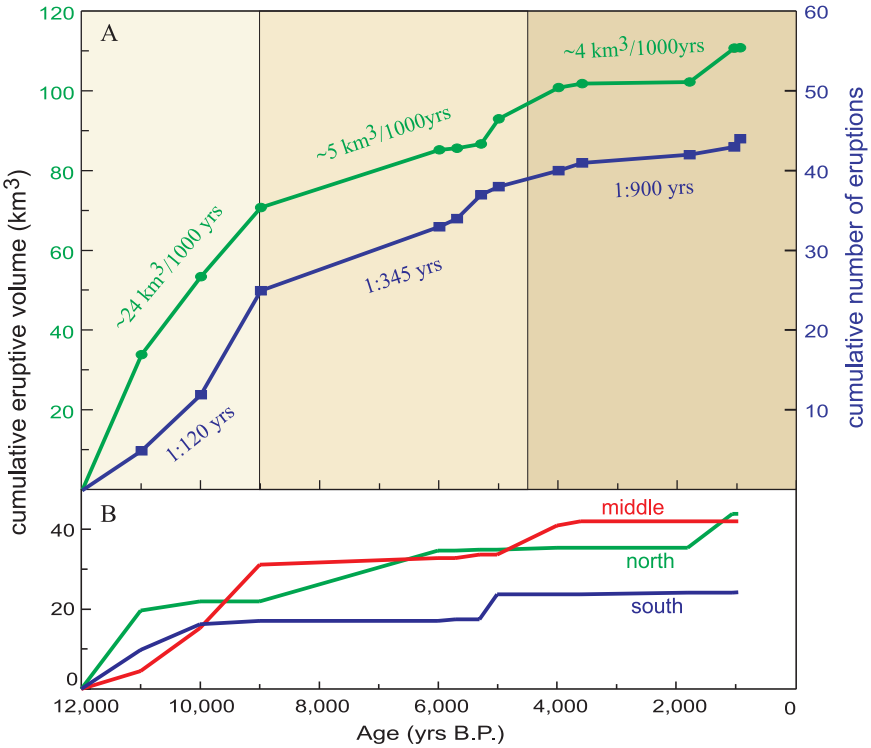


**Figure 11.** Variation in erupted volume and number of eruptions of the WVZ with time indicates a steadily decreasing production rate. About 57% of the total number of eruptions known from the WVZ occurred within the first 3000 years after deglaciation; these eruptions produced almost 64% of the total postglacial erupted volume of the WVZ. There has been a ~6-fold decrease in erupted volume and 7.5-fold decrease in eruption rate in the last 4,500 years compared to the first 3000 years following deglaciation.

possible to explain this gradient by variations in the melting process, e.g., by higher extents of total melting or preferential sampling of the shallower parts of an upwelling mantle column in the north, the most likely explanation is that the mantle source region beneath the northern WVZ is more depleted in incompatible elements. Similar relations in Plio-Pleistocene sections [*Schilling et al.*, 1982], suggests that this gradient is likely to be a long-lived feature of western Iceland asthenosphere.

[50] Lavas older than 9 Ka tend to have lower Zr/Y than younger lavas in both the northern and main WVZ populations. This result is consistent with higher extents of melting prior to 9 Ka than during later times, similar to interpretations of *Jull and McKenzie* [1996], *Slater et al.* [1998], and *Maclennan et al.* [2002] for melting maxima in response to deglaciation. This feature of WVZ volcanic history is explored further in the following section.

## 7. Temporal Variations

[51] Figure 11 shows the variation in total erupted volume and eruption frequency with age. It is clear that the WVZ has undergone steadily declining production since early postglacial time. About 57% of the total number of postglacial eruptions known from the WVZ occurred within the first 3000 years; these eruptions produced almost 64% of the total postglacial erupted volume. There has been a ~6-fold decrease in erupted volume and 7.5-fold decrease in eruption rate in the last 4,500 years compared to the first 3000 years of postglacial time.

[52] The lower panel of Figure 11 shows the partitioning of erupted volume among three regions corresponding to Figures 3 (middle), 4 (south), and 6 (north). For the whole of postglacial time the northern and middle areas have been about equally productive, producing approximately 44 km$^3$, and 42 km$^3$, respectively. In contrast, only a little more than 24 km$^3$ has been erupted south of Thingvallavatn along the WVZ over the same period. However, the southernmost part of the WVZ overlaps with volcanic segments of the Reykjanes peninsula (Figure 1), and *Jakobsson et al.* [1978] estimate that the two westernmost of these segments produced ~18 km$^3$ during postglacial time. Thus, taken together the evidence indicates no

significant along-strike variation in volcanic production in western Iceland, at least during the last ~12,000 years.

[53] The presence of production maxima in early postglacial time has been documented in every Icelandic region for which there are sufficient data, most notably on the Reykjanes Peninsula [*Jakobsson et al.*, 1978], the Veidivötn fissure swarm of the EVZ [*Vilmundardóttir and Larsen*, 1986], the Dyngjufjöll region in the southern part of the NVZ [*Sigvaldason et al.*, 1992], and the Theistareykir and Krafla regions in the northern part of the NVZ [*Slater et al.*, 1998; *Maclennan et al.*, 2002]. Previous authors have related the eruption pulse to the effects of deglaciation, although there is a lack of agreement as to whether this eruption pulse is at least partly driven by processes occurring in the mantle. There are three principal manifestations associated with the period of volcanic history immediately following ice removal. (1) an increase in eruption rate, up to 30–50 times that in the late-glacial and younger postglacial times; (2) decreases in highly incompatible to moderately incompatible element ratios of erupted lavas, and (3) wide range in MgO contents of erupted lavas, generally ranging to higher values (Figure 12). In addition, several authors have noted a dominance of central-vent, lava shield eruptions over fissure-fed eruptions in early postglacial times.

[54] *Gudmundsson* [1986] proposed a mechanical explanation for enhanced tapping of crustal magma chambers associated with increases in magmatic pressures and bending stresses during early postglacial uplift, and *Sigvaldason et al.* [1992] favored this explanation for effects observed in the Dyngjufjöll region in the southern part of the NVZ. Because ratios of incompatible elements, especially those with approximately equivalent bulk partition coefficients, are unaffected by crystal fractionation and many other crustal processes, *Hardarson and Fitton* [1997], *Slater et al.* [1998], and *Maclennan et al.* [2002] argued for increased melting rates during the period immediately following ice removal. This effect has been shown to be quantitatively consistent with theoretical predictions of *Jull and McKenzie* [1996], who showed that small increases (<1%) in extent of melting of the upper mantle can increase total magma production rates by factors of 30–50 over those during glacial or later postglacial times. Although *Gee et al.* [1998a, 1998b] argued that variations in Nb/Zr and isotopic ratios of Reykjanes Peninsula lavas could be produced entirely by crustal processes such as crystallization, assimilation, and mixing, these arguments were not supported by quantitative models. Furthermore, as emphasized by *Jull and McKenzie* [1996] and *Maclennan et al.* [2002], irrespective of the effects on crustal magma reservoirs, it is extremely difficult to prevent increases in melt production by decompression melting following glacial unloading.

[55] The most likely scenario is that rebound and enhanced decompression leads to increased melting and hence higher magma supply in early postglacial times. MgO of aphyric rocks generally correlates with magmatic temperature, which in turn can be related to magma supply [*Christie and Sinton*, 1981; *Sinton et al.*, 1991] although complications can arise from variations in magma chamber structure [*Sinton and Detrick*, 1992]. High magma supply systems have high rates of replenishment of primitive magma from the mantle, which can lead to buffering of magma reservoirs to high temperatures and high-MgO compositions. Although olivine accumulation can partly explain high MgO contents of some porphyritic lavas such as early postglacial picrites, the coincidence of a broad maximum in MgO in early postglacial times (Figure 12) [see also *Maclennan et al.*, 2002] with the period of maximum volcanic production and lowest incompatible element ratios of erupted lavas, strongly suggests that all these features can be attributed to a period of enhanced melting immediately following deglaciation.

[56] *Jull and McKenzie* [1996] showed that increases in melting associated with deglaciation should be restricted to a relatively short period, depending on the vertical velocity of melt in the mantle. *Maclennan et al.* [2002] showed that, for the melt fraction versus depth curve of *Slater et al.* [1998], eruption pulses <2 kyr are consistent with melt extraction velocities >50 m/yr. Although estimated volcanic output from the central part of the WVZ was included by *Maclennan et al.* [2002] in their analysis, our current work greatly increases the resolution of the timing of events within the WVZ and extends the observations to the entire zone.

[57] For the postglacial WVZ, both the highest eruption rates and lowest Zr/Y values are found in the earliest (finiglacial) lavas. Up until about 9000 years B.P. eruption rates remain high but gradually decreasing as average Zr/Y increases. After ~9000 years B.P., eruption rates decrease

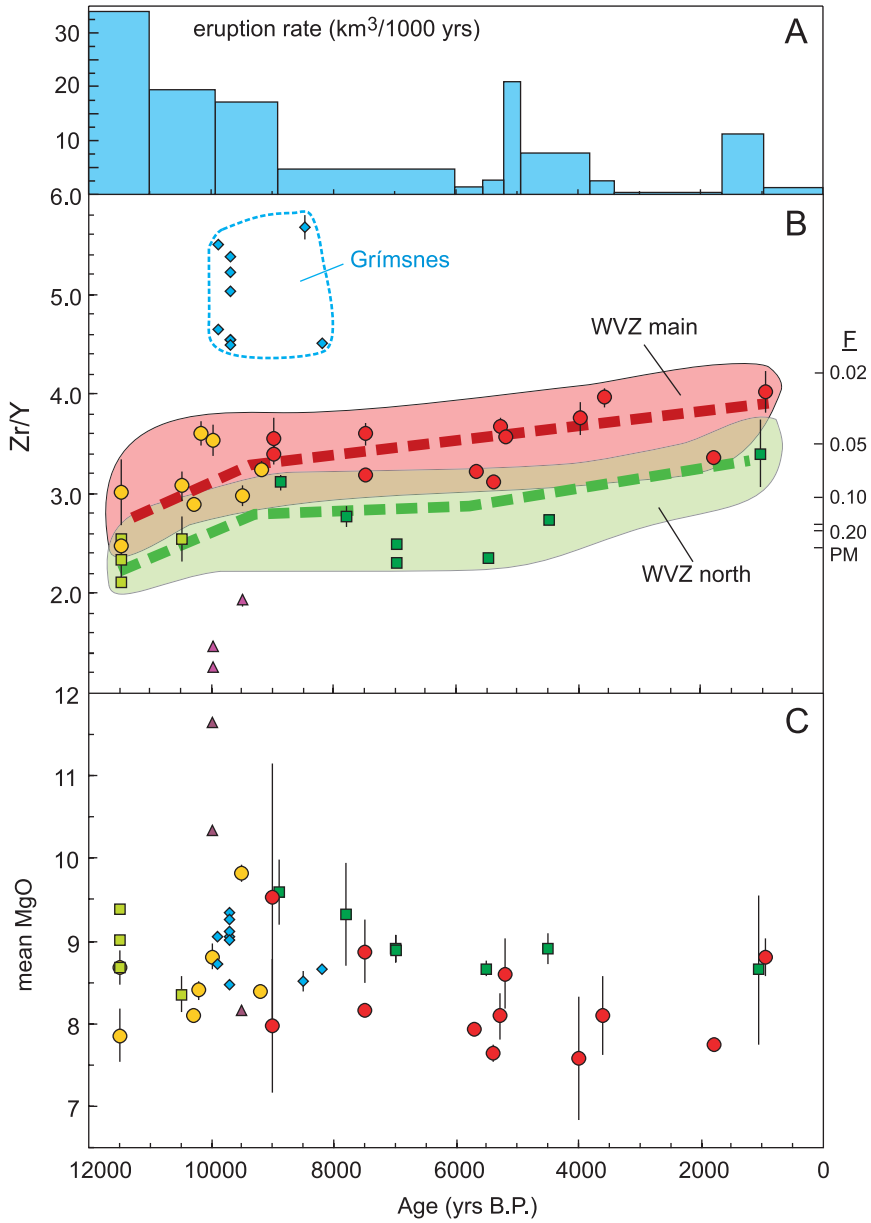


**Figure 12.** Variations in eruption rate, Zr/Y, and MgO versus age for WVZ postglacial lava units. Values in the Zr/Y and MgO panels are means for each eruptive unit ±1 σ. Sympathetic decrease in eruption rate with increasing Zr/Y in early postglacial time is consistent with high initial melting rates that decline slightly for about 3000 years. Since ~9000 years B.P., average Zr/Y has steadily increased, along with steady decline in eruption rate (Figure 11). Lavas from the northern part of the WVZ (Figure 6) have lower Zr/Y at all ages than those farther south, with the exception of those units noted in the text. This result could reflect a regional gradient of more depleted mantle composition to the north, although systematic north-south variations in melting processes cannot be ruled out by the present study.

dramatically while Zr/Y gradually increases up to the last eruptions about 1000 years ago. Relatively short-lived bursts in eruptive activity correspond to the Leitahraun, Lambahraun and Hallmundarhraun eruptions, 5200, 4000, and 1000 years ago, respectively. A broad maximum in average MgO occurs about 9000–9500 years B.P., or possibly earlier depending on whether or not one includes the picritic shields for which our age assignments are especially tentative. Taken together, these results suggest that processes directly attributable to deglaciation probably last until about 9000 years B.P., or approximately 2–3 kyr following ice removal. During this period eruption rates and Zr/Y values show rapidly varying, sympathetic relationships, consistent

with an initial pulse of high melting followed by a gradual decline.

[58] Neither the progressive decrease in eruption rate (Figure 11) nor increasing Zr/Y (Figure 12) in the period since 9 kyr is predicted by current models of the effects of deglaciation. Although our current understanding of melting processes affecting the WVZ are rudimentary, it is notable that geochemical indicators of declining extent of melting, e.g., Zr/Y, generally correlate with a decline in eruptive frequency and volcanic production. Thus the evidence from the WVZ is that this spreading center has been becoming progressively less active magmatically throughout postglacial time, a trend that continued beyond the initial period of postglacial rebound to the present day.

[59] Chemical data for lavas of the Reykjanes Peninsula [*Gee et al.*, 1998a] show strikingly similar temporal variations to those of the WVZ, particularly with respect to distinctly different behavior before and after ~9,000 years B.P., and in a gradual increase in average Nb/Zr continuing to the present. Fully comparable data with respect to eruption age are not presently available for the Northern and Eastern Volcanic Zones, although *Maclennan et al.* [2002] showed that La concentrations of 6 eruptions younger than 3000 years from Theistareykir and Krafla are significantly higher than those of 11 eruptions occurring prior to 7000 years B.P. This comparison indicates that the declining magmatic vigor exemplified by the WVZ is not restricted to that particular part of the plate boundary, but rather appears to be a feature of all of western Iceland. This result might be explained in terms of competing tectonic scenarios between eastern and western Iceland volcanic zones (see below), but the limited data from North Iceland instead suggest that declining extents of melting (and overall magmatic production) may be a regional feature of the Iceland hot spot, one that can only be fully evaluated with many more data than are presently available.

## 8. Is the Western Volcanic Zone Dying?

[60] The WVZ is the remnant of a long-lived, active plate boundary that formed about 6–7 Ma. The entire Reykjanes-Langjökull zone was the dominant plate boundary in Iceland up until 1.5–3 Ma, when plates in south Iceland began to reorganize toward the present configuration [*Sæmundsson*, 1979; *Sæmundsson and Jóhannesson*, 1994]. Once the EVZ formed, spreading along the plate boundary in south Iceland became partitioned between the WVZ and EVZ, the two subparallel rifts that form margins of the south Iceland microplate (Figure 1). Present-day extension along the WVZ is about 20–30% of the total plate separation in south Iceland. *Jakobsson* [1979] estimated the total postglacial lava production of the EVZ to be slightly greater than 200 $km^3$, or about 80% greater than our estimate of that along the WVZ.

[61] Because the EVZ dominates the extension and volcanic production in south Iceland, and because it formed relatively recently, some authors have speculated that the EVZ will eventually replace the WVZ as the sole plate boundary in southern Iceland [*Pálmason*, 1981; *Schilling et al.*, 1982; *Óskarsson et al.*, 1985; *Meyer et al.*, 1985; *Einarsson*, 1991], in a process akin to rift propagation [*Hey et al.*, 1980]. In this scenario, the WVZ is the failing or dying rift, the EVZ is the propagating rift, and the SISZ (Figure 1) would be the migrating transform zone. When the NVZ formed, it did so at the expense and total extinction of the northern continuation of the Reykjanes-Langjökull zone [*Sæmundsson*, 1979], similar to the discontinuous propagating rift model of *Hey et al.* [1989]. However, the more recent formation of the EVZ did not completely replace the remaining WVZ.

[62] If the entire system propagates and fails discontinuously, then the present microplate configuration could be stable until the next phase of discontinuous propagation and associated failure in the west. However, evidence for continuing southward propagation of the EVZ includes an age progression in the flanking Plio-Pleistocene section east of it [*Sæmundsson and Jóhannesson*, 1994] and the recent arrival of tholeiitic magma into Torfajökull to the south [*Sæmundsson and Friðleifsson*, 2001]. Thus the recent evolution of the EVZ appears to be consistent with the continuous propagation model [*Hey et al.*, 1989].

[63] Despite the evidence for continued southward propagation of the EVZ we have found no evidence in the postglacial volcanic record for progressive failure of the WVZ. If rift failure is continuous then the WVZ should be progressively dying from north to south. However, according to our data, the northern part of the WVZ has been at least as productive in postglacial time as the rest of the WVZ. Most likely the northern part of the WVZ has been even more productive than farther south, considering that we have been able to estimate only part of the production from vents

**Table 6.** Volcanic Morphology of the Western Volcanic Zone[a]

| | Fissure Eruptions | Central-Vent Eruptions | |
|---|---|---|---|
| | >1 km length | Small Shields and Cones | Lava Shields |
| | krt | kkh | hmh |
| | nsh | sfh | lbh |
| | tfh | hfh | lth |
| | hvh | sth | kjh |
| | shh | gbh | glh |
| | ebh | bsh | sk-II |
| | | tjh | svh |
| | | + 10 Grímsnes | dda |
| | | | bfh |
| | | | hhh |
| | | | hfs |
| | | | lgh |
| Median volume, km$^3$ | 0.40 | 0.54[b] | 6.3 |

[a] Unit designations are those of Table 3. Small shields have summit cones, without a well-developed summit crater.
[b] Volume for small shields does not include data for Grímsnes lava units.

currently buried beneath Langjökull. Furthermore, the Hofsjökull Zone is a very large and productive volcanic center, which is not consistent with a failing rift system. The overall decline in volcanic production and increase in incompatible element ratios of the WVZ in the last 9000 years appears to be a widespread feature in Iceland, and therefore not apparently related to plate boundary reorganizations. One characteristic of failing rifts at slow and intermediate spreading rates is the development of deep graben structures [e.g., *Hey et al.*, 1989], and the Thingvellir depression is the deepest graben structure in Iceland. Again, however, the northern WVZ is the least faulted of any part of the volcanic zone and a region where volcanism appears to clearly dominate over tectonic processes. The WVZ has shown significant activity within postglacial time, most recently in 1789 A.D. [*Sæmundsson*, 1990, 1992].

[64] The type example of a propagating/failing rift system is the Galápagos spreading center near 95°W, a region with vastly lower overall magma supply than in Iceland. Nevertheless, the evidence from the Galápagos region indicates that the eastern rift is propagating continuously while the western rift is failing discontinuously [*Hey et al.*, 1989]. Although the observations along the WVZ presented here pertain only to the short period of postglacial time, the lack of evidence for short-term rift failure along the WVZ may indicate a similarity to the Galápagos 95°W system, i.e., continuous southward rift propagation of the EVZ associated with discontinuous failure in the west, even though the scale of failed rifts in west Iceland is several times larger than the failed rift segments of the Galápagos system. Clearly the ultimate understanding of the tectonic evolution of south Iceland will require a much better understanding of the accretionary history of both the WVZ and EVZ over several hundred thousand to millions of years, and not just the relatively short interval since the last major glaciation.

## 9. Eruption Style in Icelandic Volcanic Zones

[65] Volcanic eruptions in the Western Volcanic Zone can be generally classified into fissure eruptions and central vent eruptions. Central-vent volcanoes of the WVZ include large lava shields, typically characterized by a summit crater more that 100 m in diameter, and smaller shield structures typically characterized by one or more cones concentrated in the summit region, with or without a summit crater. These latter edifices range from small spatter cones to much larger cinder cones. WVZ eruptions fed by large cinder cones are confined to the early postglacial Tjarnahnúkur eruption, and some of the eruptions in the Grímsnes flank field, including the Seyðishólar/Kerhóll eruption, the largest in that field. Of the 44 known eruptive units in the WVZ, most can be unambiguously classified according to the scheme shown in Table 6. Significant proportions of the outcrop areas including vent structures of the other nine units are now buried by younger extrusives and are therefore not included in Table 6. However, five of those consist of compound lava [*Walker*, 1971] and these units almost certainly represent partially buried flanks of lava shields. The principal differences

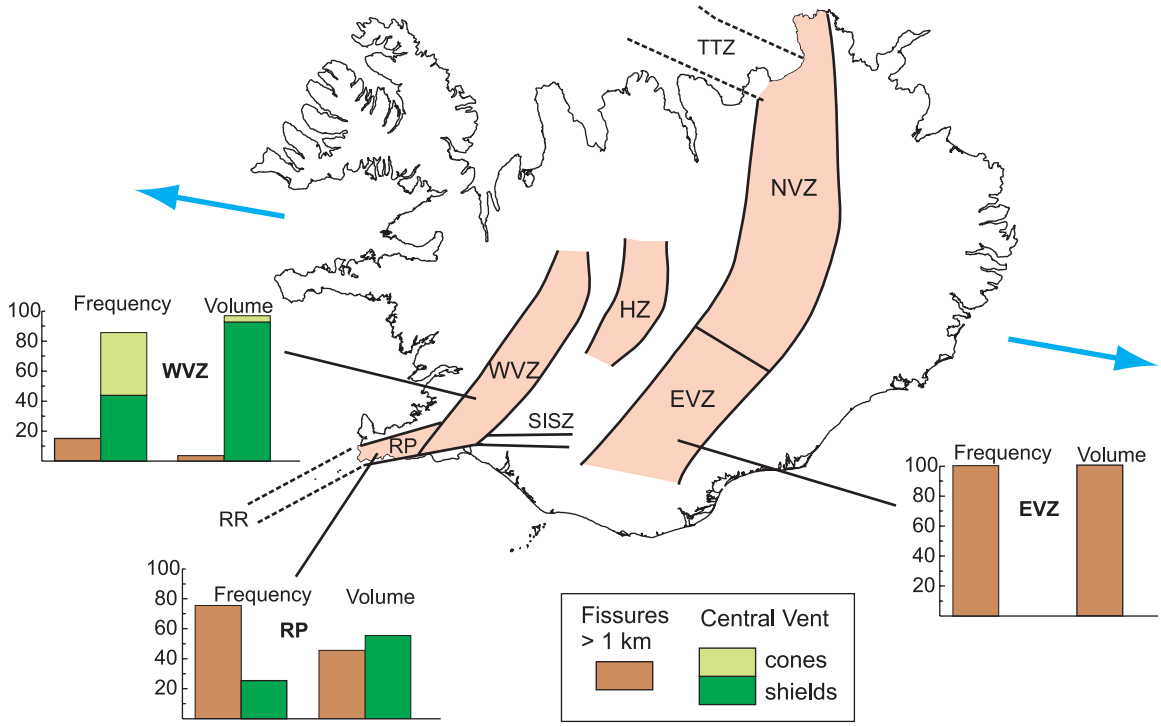


**Figure 13.** Generalized map of Iceland showing the principal plate boundary zones. Histograms show the relative proportions of central-vent and fissure-fed lava eruptions in the Reykjanes Peninsula (RP; data from *Jakobsson et al.* [1978]), Western Volcanic Zone (WVZ; this study), and Eastern Volcanic Zone (EVZ; data from *Jakobsson* [1979]); frequency histograms show the distribution by number of eruptions, while volume histograms show the distribution scaled to the volume of lava produced by the two main types of eruption. Although comparable data are not presently available for the NVZ, mapping indicates approximately equal proportions of fissure and shield volcanoes, similar to that of the Reykjanes Peninsula. Blue arrows show the overall spreading direction according to Nuvel 1A [*DeMets et al.*, 1994].

between cone-fed eruptive units and lava shields are size and presence of summit craters. Most likely cone-fed units would have developed into lava shields had the eruptions lasted longer [*Rossi*, 1996]. Thus we include small shields with summit cones along with more classic lava shields into the general category of central-vent volcanoes.

[66] We have included the Hallmundarhraun eruption within the central vent category in Table 6, despite having as many as 4 separate vents spread over a distance of ~18 km. We find no evidence for continuous fissures between these vents and the great majority of lava was produced from isolated vents at low effusion rates, producing broad shield structures and compound pāhoehoe lava, characteristics typical of lava shields. Although this eruption may have initiated along a long fissure, the later stages were clearly concentrated along one or more centrally fed vents.

[67] Postglacial activity along the WVZ has been dominated by central vent activity. Only 6 units are known to have been erupted from fissures longer than ~1 km. All of these are younger than about 8000 years old, and all are comparatively small volume. Thus fissure eruptions constitute about 15% of the known eruptions, but these eruptions account for less than 4% of the total volume erupted in postglacial time. However, fissure eruptions have been very common in more recent times; at least 3 of the last 4 eruptions were fissure eruptions, depending on how one classifies the Hallmundarhraun eruption.

[68] The nature of volcanic activity in the WVZ contrasts markedly with that in other volcanic zones (Figure 13). Along the Reykjanes Peninsula fissure eruptions are much more numerous than along the WVZ, and volume production is about evenly split between fissure and shield eruptions [*Jakobsson et al.*, 1978]. Even more striking is the complete lack of lava shields in the EVZ [e.g., *Sæmundsson*, 1978; *Jakobsson*, 1979]. Fully comparable data are not yet available from the NVZ, but it is known that the eruptive products there are about evenly distributed between lava shields and

eruptive fissures for the entire zone throughout postglacial time. However, some parts of the NVZ are exclusively characterized by lava shields, e.g., Theistareykir, whereas the last three major eruptive episodes along the NVZ are all fissure eruptions. Thus the overall distribution of eruptive style in the NVZ more closely resembles that of the Reykjanes Peninsula than either the WVZ or EVZ.

[69] There are major differences in opening rate, degree of obliquity and overall magma supply among the principal volcanic zones of Iceland. Although the WVZ and EVZ represent extremes in volcanic style, neither is an end-member in any of these tectonic variables. The Reykjanes Peninsula is the most oblique plate boundary in Iceland, whereas the NVZ has a higher opening rate than either the WVZ or EVZ, where the full plate separation is partitioned between the two extensional zones that bound the microplate. One measure of overall magma supply is crustal thickness, but it is notable that lava shields are present in the southern part of the NVZ close to the center of the hot spot, but not in the EVZ immediately to the south of Vatnajökull. These two regions have approximately equal crustal thickness [*Allen et al.*, 2002], and hence overall magma supply from the mantle is not significantly different in these two regions. Indeed, according to *Allen et al.* [2002], crustal thickness estimates for most of the EVZ and WVZ are not significantly different from each other. Thus explanations for the vastly different eruptive styles throughout Iceland do not seem to be related to simple tectonic comparisons among the different volcanic zones.

[70] Within the WVZ, there is a correlation among eruption type and median erupted volume (Table 6), and also lava morphology and vent structure. Fissure-fed lavas tend to have the lowest volumes and contain a higher proportion of ‘a‘ā lava, which is known to form at relatively high effusion rates [e.g., *Rowland and Walker*, 1990]. In contrast, the large-volume lava shields tend to be dominated by dense pāhoehoe, which forms at very low effusion rates. Thus eruption durations for lava shields (several tens of decades for the larger ones) are probably orders of magnitude longer than those for fissure eruptions. Although some very large fissure eruptions are known from the EVZ, these probably had high average effusion rates (see below), and eruption durations spanning only a few months to years. The relationship between edifice morphology and eruption duration is consistent with commonly observed eruption chronologies in Hawai‘i and elsewhere [e.g., *Richter et al.*, 1970; *Thorarinsson et al.*, 1973; *Lockwood et al.*, 1987], as well as with models of lava shield evolution [*Rossi*, 1996]. Eruptions that begin as fissure-fed lava flows might ultimately close down to a small number of eruptive centers with diminishing eruption rates. Well-developed lava shields are the end result of long-lived eruptions characterized by overall low average effusion rates.

## 9.1. Large-Volume Eruptions: A Tale of Two Volcanoes

[71] The size of a volcanic eruption reflects competing processes of magma availability and cooling processes [e.g., *Head et al.*, 1996]. An over-riding limit to the size of an eruption is the amount of magma available during an eruptive episode, i.e., a supply limitation. However, magma availability can be considered to reflect two contrasting sources: the amount of magma stored up in crustal (or mantle) reservoirs prior to eruption, and the amount of new, mantle-derived (recharge) magma being supplied to the reservoir during the eruption. In this way, large-volume eruptions can be accommodated in two ways, (1) tapping of very large magma reservoirs, or (2) tapping reservoirs at a rate approximating the rate of recharge of new magma from below. These two ‘‘classes’’ of large-volume eruptions can be expected to differ in a number of characteristics. For example, recharge controlled eruptions will have low effusion rates, ultimately limited by the rate at which magma can arise out of the mantle. They also are likely to be chemically heterogeneous and generally high in Mg because of limited crustal residence. In contrast the effects of prolonged residence in large magma chambers should result in generally more homogeneous magma with lower Mg contents, and large magma chamber eruptions can have eruption rates that are not dependent on the rates of resupply of new magma from the mantle.

[72] Two very large eruptions, one of them among the best known in Iceland, serve to illustrate these points. The Skjaldbreiður lava shield of the WVZ and the Laki lava of the EVZ have similar large volumes (Figure 14). Laki lava was erupted from a long fissure over a period of about 8 months [*Thordarson et al.*, 1996], whereas the Skjaldbreiður shield is composed almost entirely of dense pāhoehoe lava. Assuming an average effusion rate of $\sim$5–10 $m^3$/sec for this lava [*Rowland and Walker*, 1990; *Rossi*, 1996], it was erupted over a

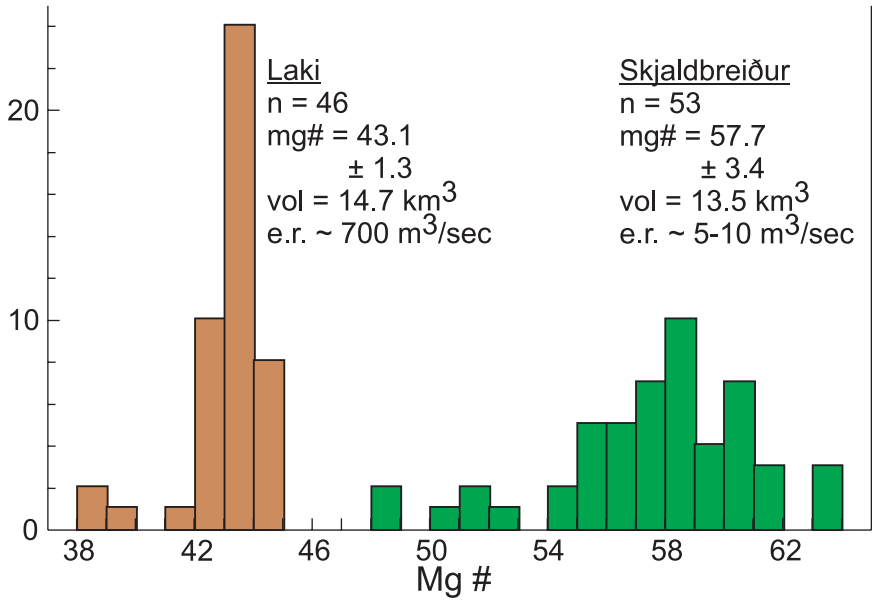


**Figure 14.** Mg # (100 Mg/(Mg + total Fe) histograms for Laki and Skjaldbreiður. Vertical axis is number of analyses (n). For each flow field total number of analyses (n), average Mg # ±1 σ, total erupted volume (vol.; Laki data from *Thordarson et al.* [1996]), and eruption rate (e.r.) are given. Eruption rate for Laki is the volume divided by the known eruption duration (~8 months); eruption rate for Skjaldbreiður is inferred from studies of lava morphology [*Rowland and Walker*, 1990; *Rossi*, 1996]. Laki chemical data from *Grönvold* [1984], *Thordarson et al.* [1996], and unpublished data of T. Thordarson (personal communication, 2005). Skjaldbreiður data from this study, including samples analyzed at University of Hawai'i (xrf) and Nordic Volcanological Institute (ICP). Compared to Skjaldbreiður, Laki is much more homogeneous at significantly lower Mg #. The relative homogeneity of Laki lava is apparent despite the inclusion of data from several different laboratories and analytical methods in the compilation.

period of about 40–80 years. Skjaldbreiður lava is chemically heterogeneous over a range of moderately high MgO; we presented evidence earlier in this paper that the nature of the trace element heterogeneity of this unit requires the composition of parental magma, i.e., that being fed from the mantle, to have varied during the course of the ongoing eruption. Thus Skjaldbreiður is a good example of a lava shield formed by a long-lived eruption, one that owes its longevity to sustained but slow mantle recharge. In contrast, Laki lava is much more homogeneous and much more differentiated, indicating significant crustal residence prior to eruption. It is an example of a large-volume, moderately homogeneous, high-effusion rate eruption, all features that can be explained by eruption from a large crustal magma chamber that did not require significant recharge during the course of the eruption.

## 9.2. Variations in Space and Time

[73] The temporal variation within the WVZ can be explained in terms of the overall decline in magma supply during postglacial time. In the early postglacial, when rebound-induced melting rates were at a maximum, the probability for mantle recharge-sustained eruptions also was maximized. Although many eruptions may have begun as fissure-fed eruptions, long-lived lava shields sustained by recharge dominate the early postglacial period. Significant mantle recharge during these eruptions also explains the MgO maximum characteristic of this period. In later postglacial times relatively short-lived fissure eruptions have become increasingly common. Only a few of these later eruptions were sustained by replenishment during eruption, most notably the moderately large-volume lava shields of Lambahraun and Hallmundarhraun. The lack of evidence for large-volume fissure-fed eruptions anywhere along the WVZ suggests that large magma chambers have been rare or absent in the WVZ for most of postglacial time.

[74] Differences between volcanic zones are less easily accounted for, but the lack of shield volcanoes in the EVZ suggests that long-lived eruptions have not occurred there. Although some very large volume eruptions have taken place, these were accompanied by average effusion rates high enough to prevent closing down of eruptive fissures to central vents. Thus our interpretations suggest that

large crustal magma chambers have been, at least intermittently, present beneath parts of the EVZ. Why these reservoirs might erupt with high average effusion rates is not clear from presently available data. *Thordarson et al.* [1996, 2003] demonstrated that high volatile content is a characteristic of EVZ volcanic systems, and high volatile contents can be expected to contribute to magma driving pressures and thereby increase average effusion rates [*Wilson and Head*, 1981; *Vergniolle and Jaupart*, 1986]. Comparable data are not presently available for WVZ magmas, but *Unni and Schilling* [1978] and *Schilling et al.* [1983] showed that the Iceland plume is halogen- and $H_2O$-rich and, because the EVZ is closer to the center of the Iceland plume than is the WVZ, one might expect higher volatile contents to the east, which in turn, might drive high effusion rate eruptions.

## 10. Conclusions

[75] Through a combination of field observations, new age constraints, and extensive chemical analysis, we have been able to refine the details of postglacial eruptive history in space and time along the 170-km-long Western Volcanic Zone to unprecedented resolution. We have identified 44 separate eruptive units, 10 of which are small-volume eruptions associated with the flanking Grímsnes volcanic field. Five of the 34 units in the main part of the WVZ were not recognized by previous work, while outcrop areas and ages of several others have been revised. The distribution of eruptive centers and associated normal faults and fissures locally define well-developed volcanic segments, especially in the southern part of the WVZ. To the north the overall zone is more than 25 km wide and the distribution of centers is more diffuse.

[76] Five eruptive units show evidence for interaction with significant volumes of ice or meltwater and therefore probably formed at the end of the last glaciation. An additional 11 units formed prior to ~9000 years B.P. The 16 eruptions in the first 3000 years of postglacial time account for about 64% of the total postglacial production, consistent with varying production rates elsewhere in Iceland, which have been ascribed to enhanced melting and/or enhanced eruptibility as a consequence of rebound immediately following deglaciation. Incompatible element compositions of WVZ magmas are consistent with enhanced melting in the first 3000 years of postglacial time. High MgO at this time probably reflects a combination of overall high magma supply and the propensity for long-duration lava shield eruptions that were being recharged from the mantle during the course of the eruptions.

[77] Overall chemical variations within the WVZ are consistent with very simplified models of melting of a source approximating primitive mantle composition, without requiring selective enrichment in Nb. We agree with previous work that dynamic melting processes appear to be required to account for a number of features of the chemical variation, including the presence of lavas that are highly depleted in incompatible elements, although a more realistic appraisal of multicomponent source melting processes is beyond the scope of this paper. Steadily declining eruption rates throughout postglacial time correlate with changes in average incompatible element ratios that appear to reflect continued decline in melting extents to the present day. This result is not restricted to the WVZ, however, and may herald a long-term decline in melting associated with the Iceland hot spot. Superposed on the temporal trends in chemical composition is a strong spatial variation. Lavas from the northern part of the WVZ are depleted in incompatible elements relative to those from the south at all times. Whether this result reflects a long-wavelength gradient in mantle source composition or variations in the melting process along axis, is not yet clear.

[78] Since ~1.5–3 Ma, spreading in south Iceland has been partitioned between two spreading centers, the EVZ and WVZ, on either side of a microplate. Recent measurements suggest that about 20–30% or less of the spreading is occurring on the WVZ, making this the slowest spreading, magmatically active plate boundary currently known. Sparse evidence suggests that the tectonic evolution of south Iceland is consistent with continuous propagation of the EVZ accompanied by discontinuous failure of western spreading zones. There is no evidence for along-strike variations in volcanic productivity during postglacial time, which would be predicted by a failing rift hypothesis. A low in volcanic production in the area of Lake Thingvallavatn is more than balanced by high production farther to the NE. Other structural features that might be expected to accompany rift failure also are lacking over the short period of postglacial activity of this study.

[79] Eruptive activity along the WVZ has been dominated by the production of lava shields. Only 4% of the total volume was erupted from fissures,

although 3 of the last 4 eruptions were fissure eruptions. The eruptive character of the WVZ contrasts markedly with that of the Reykjanes Peninsula and especially the EVZ, where lava shields are entirely lacking. The key variables distinguishing shield and fissure eruptions are average effusion rate and eruption duration, both within the WVZ and between different volcanic zones. These variables, in turn, can be related to the source of magma during single eruptions. Those eruptions that are sustained by slow recharge of new magma from the mantle will erupt with low average effusion rates, and tend to be relatively heterogeneous chemically with overall high Mg contents. These are characteristics of many WVZ lava shields. In contrast, those eruptions that tap crustal magma reservoirs will be less variable chemically at overall lower Mg contents, and can erupt with much higher average effusion rates. These are characteristics of fissure eruptions from both the WVZ and at least some of those from the EVZ and probably elsewhere. High effusion rate, large volume eruptions require the presence of large crustal magma reservoirs, which have been rare or absent in the WVZ throughout postglacial time.

## Acknowledgments

[80] This material is based upon work supported by the National Science Foundation, under grants OCE 98-11276 and INT 99-10570, and the Nordic Volcanological Institute. J.S. is grateful to the late Gudmundur Sigvaldason for his encouragement and support in the early stages of this work. Eric Bergmanis, Buffy Cushman, Gretar Ívarsson, Haukur Jóhannesson, Todd Presley, Ken Rubin, JoAnn Sinton, Anna Dis Sveinbjörnsdóttir, Sigurlaug Sveinbjörnsdóttir, and Iris van der Zander helped with various aspects of the field mapping. Rósa Ólafsdóttir provided hand-digitized topographic contours for much of the WVZ; Scott White and Nathan Becker helped with the production of some of the maps presented in this paper. We are grateful to Thorvaldur Thordarson for allowing us to use unpublished whole rock data for the Laki lava flow, to Helgi Björnsson for providing a prepublication image of the topography beneath Langjökull, and to Ómar Bjarki Smárason of Stapi Ltd. for access to cores from the Thorlákshöfn area. This work has benefited greatly from discussions with Richard Hey, Niels Óskarsson, Ken Rubin, Freysteinn Sigmundsson, Thorvaldur Thordarsson, and Iris van der Zander and formal reviews of an earlier version of the manuscript by Cristophe Hémond and Godfrey Fitton. This is SOEST contribution 6658.

## References

Allen, R. M., et al. (2002), Plume-driven plumbing and crustal formation in Iceland, *J. Geophys. Res.*, *107*(B8), 2163, doi:10.1029/2001JB000584.

Áskelsson, J. (1953), Nokkur orð um íslenzkan fornfugl og fleira, *Náttúrufræðingurinn*, *23*, 133–137.

Bernauer, F. (1943), Junge Tektonik auf Island und ihre Ursachen, in *Spalten auf Island*, edited by O. Niemczyk, pp. 14–64, K. Wittwer, Stuttgart, Germany.

Björnsson, A. (1985), Dynamics of crustal rifting in NE Iceland, *J. Geophys. Res.*, *90*, 10,151–10,162.

Bull, J. M., T. A. Minshull, N. C. Mitchell, K. Thors, J. K. Dix, and A. I. Best (2003), Fault and magmatic interaction within Iceland's western rift over the last 9 kyr, *Geophys. J. Int.*, *154*, 1–8.

Chauvel, C., and C. Hémond (2000), Melting of a complete section of recycled oceanic crust: Trace element and Pb isotopic evidence from Iceland, *Geochem. Geophys. Geosyst.*, *1*(2), doi:10.1029/1999GC000002.

Christie, D. M., and J. M. Sinton (1981), Evolution of abyssal lavas along propagating segments of the Galapagos Spreading Center, *Earth Planet. Sci. Lett.*, *56*, 321–335.

DeMets, C., R. G. Gordon, D. F. Argus, and S. Stein (1994), Effect of recent revisions to the geomagnetic reversal time scale on estimates of current plate motions, *Geophys. Res. Lett.*, *21*, 2191–2194.

Devey, C. W., C.-D. Garbe-Schoenberg, P. Stoffers, C. Chauvel, and D. F. Mertz (1994), Geochemical effects of dynamic melting beneath ridges: Reconciling major and trace element variations in Kolbeinsey (and global) mid-ocean ridge basalt, *J. Geophys. Res.*, *99*, 9077–9095.

Dick, H. J. B., J. Lin, and H. Schouten (2003), An ultraslow-spreading class of ocean ridge, *Nature*, *426*, 405–412.

Dugmore, A. J., G. T. Cook, J. S. Shore, A. J. Newton, K. J. Edwards, and G. Larsen (1995), Radiocarbon dating tephra layers in Britain and Iceland, *Radiocarbon*, *37*, 379–388.

Einarsson, P. (1991), Earthquakes and present-day tectonism in Iceland, *Tectonophysics*, *189*, 261–279.

Einarsson, P., and K. Sæmundsson (1987), Earthquake epicenters 1982–1985 and volcanic systems in Iceland, map, Menningarsjóður, Reykjavík.

Einarsson, Th. (1960), Thættir úr jardfraedi Hellisheidar, *Náttúrufræðingurinn*, *30*, 151–175.

Elliot, T., C. J. Hawkesworth, and K. Grönvold (1991), Dynamic melting of the Iceland plume, *Nature*, *351*, 201–206.

Fitton, J. G., A. D. Saunders, M. J. Norry, B. Hardarson, and R. N. Taylor (1997), Thermal and chemical structure of the Iceland plume, *Earth Planet. Sci. Lett.*, *153*, 197–208.

Fitton, J. G., A. D. Saunders, P. D. Kempton, and B. S. Hardarson (2003), Does depleted mantle form an intrinsic part of the Iceland plume?, *Geochem. Geophys. Geosyst.*, *4*(3), 1032, doi:10.1029/2002GC000424.

Gee, M. A., R. N. Taylor, M. F. Thirlwall, and B. J. Murton (1998a), Glacioisotacy controls chemical and isotopic characteristics of tholeiites form the Reykjanes Peninsula, SW Iceland, *Earth Planet. Sci. Lett.*, *164*, 1–5.

Gee, M. A., M. F. Thirlwall, R. N. Taylor, D. Lowry, and B. J. Murton (1998b), Crustal processes: Major controls on Reykjanes Peninsula lava chemistry, SW Iceland, *J. Petrol.*, *39*, 819–839.

Govindaraju, K. (1994), 1994 compilation of working values and sample description for 383 geostandards, *Geostand. Newsl.*, *18*, 1–158.

Grönvold, K. (1984), Bergfræði Skaftáreldahrauns (The Petrochemistry of the Laki lava flow), in *Skaftáreldar 1783–1784: Ritgerdir og Heimildir*, edited by G. A. Gunnlaugsson, pp. 49–58, Mál og Menning, Reykjavík.

Gudmundsson, A. (1986), Mechanical aspects of postglacial volcanism and tectonics of the Reykjanes Peninsula, Southwest Iceland, *J. Geophys. Res.*, *91*, 12,711–12,721.

Gudmundsson, A. (1987a), Geometry, formation and development of tectonic fractures on the Reykjanes Peninsula, Southwest Iceland, *Tectonophysics*, *139*, 295–308.

Gudmundsson, A. (1987b), Tectonics of the Thingvellir fissure swarm, SW Iceland, *J. Struct. Geol.*, *9*, 61–69.

Gudmundsson, A., and K. Bäckström (1991), Structure and development of the Sveinagja graben, Northeast Iceland, *Tectonophysics*, *200*, 111–125.

Guðmundsson, M. T., Th. Högnadóttir, and S. P. Jakobsson (2000), Hraun og móbergsmyndanir sunnan Langjökuls nidurstödur Thyngdarmælinga, *RH-28-2000*, 37 pp., Raunvísindastofnun Háskólans, Reykjavík.

Hanan, B. B., and J.-G. Schilling (1997), The dynamic evolution of the Iceland mantle plume: The lead isotope perspective, *Earth Planet. Sci. Lett.*, *151*, 43–60.

Hardardóttir, J., Á. Geirsdóttir, and T. Thordarson (2001), Tephra layers in a sediment core from Lake Hestvatn, southern Iceland: Implications for evaluating sedimentation processes and environmental impacts on a lacustrine system caused by tephra fall deposits in the surrounding watershed, *Spec. Publ. Int. Assoc. Sedimentol.*, *30*, 225–246.

Hardarson, B. S., and J. G. Fitton (1997), Mechanisms of crustal accretion in Iceland, *Geology*, *25*, 1043–1046.

Head, J. W.III, L. Wilson, and D. K. Smith (1996), Mid-ocean ridge eruptive vent morphology and substructure, *J. Geophys. Res.*, *101*, 28,265–28,280.

Hémond, C., N. T. Arndt, U. Lichtenstein, and A. W. Hofmann (1993), The heterogeneous Iceland plume: Nd-Sr-O isotopes and trace element constraints:, *J. Geophys. Res.*, *98*, 15,833–15,850.

Hey, R. N., F. K. Duennebier, and W. J. Morgan (1980), Propagating rifts on mid-ocean ridges, *J. Geophys. Res.*, *85*, 2647–2658.

Hey, R. N., J. M. Sinton, and F. K. Duennebier (1989), Propagating rifts and spreading centers, in *The Eastern Pacific Ocean and Hawaii*, vol. N, edited by E. D. Winterer, D. M. Hussong, and R. W. Decker, pp. 161–176, Geol. Soc. of Am., Boulder, Colo.

Hofmann, A. W. (1988), Chemical differentiation of the Earth: The relationship between mantle, continental crust, and oceanic crust, *Earth Planet. Sci. Lett.*, *90*, 297–314.

Hospers, J. (1953), Reversals of the main geomagnetic field. I, *Proc. Acad. Sci. Amsterdam, Ser. B*, *56*, 467–476.

Jakobsson, S. P. (1966), The Grímsnes lavas, SW Iceland, *Acta Nat. Island.*, *2*, 6–30.

Jakobsson, S. P. (1976), Aldur Grímsneshrauna, *Náttúrufræðingurinn*, *46*, 153–162.

Jakobsson, S. P. (1979), Petrology of recent basalts of the Eastern Volcanic Zone, Iceland, *Acta Nat. Island.*, *26*, 1–103.

Jakobsson, S. P., J. Jonsson, and F. Shido (1978), Petrology of the western Reykjanes Peninsula, *J. Petrol.*, *19*, 669–705.

Jakobsson, S. P., G. L. Johnson, and J. G. Moore (2000), A structural and geochemical study of the Western Volcanic Zone, Iceland: Preliminary results, *InterRidgeNews*, *9*, 27–33.

Jóhannesson, H. (1980), Evolution of the rift zones in western Iceland, *Náttúrufræðingurinn*, *50*, 13–31.

Jóhannesson, H. (1989), Aldur Hallmundarhrauns í Borgarfirði, *Fjölrit Náttúrufraeðistofnunar*, *9*, 12 pp.

Jóhannesson, H., and K. Saemundsson (1998), Geologic map of Iceland, 1:500,000, Bedrock Geology, 2nd ed., Icelandic Inst. of Nat. Hist., Reykjavík.

Johnson, K. T. M., H. J. B. Dick, and N. Shimizu (1990), Melting in the oceanic upper mantle: An ion microprobe study of diopsides in abyssal peridotites, *J. Geophys. Res.*, *95*, 2661–2678.

Jónsson, J. (1971), Hraun í nágrenni Reykjavíkur, 1. Leitarhraun, *Náttúrufræðingurinn*, *41*, 49–63.

Jónsson, J. (1975), Nokkrar aldursákvaðanir, *Náttúrufræðingurinn*, *45*, 27–30.

Jónsson, J. (1977), Reykjafellsgigir og Skarðsmýrarhraun á Hellisheiði, *Náttúrufræðingurinn*, *47*, 17–26.

Jónsson, J. (1978), Geology of Reykjanes, *Orkustofnun Jarðhitadeild 7831*, 303 pp., Reykjavík.

Jónsson, J. (1979), Kristnitökuhraunid (On the age of the Svinahraun lava flow), *Náttúrufræðingurinn*, *49*, 46–50.

Jónsson, J. (1983), Eldgos á sögulegum tíma á Reykjanesskaga, *Náttúrufræðingurinn*, *52*, 127–139.

Jónsson, J. (1989), Hveragerði og nágrenni Jarðfræðilegt yfirlit, *Rannsóknastofnunin Neðri Ás*, *50*, 1–30.

Jull, M., and D. McKenzie (1996), The effect of deglaciation on mantle melting beneath Iceland, *J. Geophys. Res.*, *101*, 21,815–21,828.

Kempton, P. D. F., J. G. Fitton, A. D. Saunders, G. M. Nowell, R. N. Taylor, B. S. Hardarson, and G. Pearson (2000), The Iceland mantle plume in space and time: A Sr-Nd-Pb-Hf study of the North Atlantic rifted margin, *Earth Planet. Sci. Lett.*, *177*, 255–271.

Kjartansson, G. (1964a), Aldur nokkura hrauna á Suðurlandi ($^{14}$C ages of some postglacial lavas in South Iceland), *Náttúrufræðingurinn*, *34*, 101–113.

Kjartansson, G. (1964b), Ísladarlok og eldfjöll á Kili, *Náttúrufræðingurinn*, *34*, 9–38.

Kjartansson, G. (1966a), Nokkrar nýjar C14–aldursákvaðanir, *Náttúrufræðingurinn*, *36*, 126–141.

Kjartansson, G. (1966b), Stapakenningin og Surtsey, *Náttúrufræðingurinn*, *36*, 1–34.

Kjartansson, G. (1983), Geological map of Iceland, 1:250,000, Sheet 5, Central Iceland, Iceland Mus. of Nat. Hist., Reykjavík.

LaFemina, P. C., T. H. Dixon, R. Malservisi, T. Árnadóttir, E. Sturkell, F. Sigmundsson, and P. Einarsson (2005), Geodetic GPS measurements in south Iceland: Strain accumulation and partitioning in a propagating ridge system, *J. Geophys. Res.*, *110*, B11405, doi:10.1029/2005JB003675.

Langmuir, C. H., J. F. Bender, A. E. Bence, G. N. Hanson, and S. R. Taylor (1977), Petrogenesis of basalts from the FAMOUS area, Mid-Atlantic Ridge, *Earth Planet. Sci. Lett.*, *36*, 133–156.

Larsen, G., and S. Thórarinsson (1978), $H_4$ and other acid Hekla layers, *Jökull*, *27*, 28–46.

Lockwood, J. P., J. J. Dvorak, T. T. English, R. Y. Koyanagi, A. T. Okamura, M. L. Summers, and W. R. Tanigawa (1987), Manua Loa 1974–1984: A decade of intrusive and extrusive activity, *U.S. Geol. Surv. Prof. Pap.*, *1350*, 537–570.

Maclennan, J., M. Jull, D. McKenzie, L. Slater, and K. Grönvold (2002), The link between volcanism and deglaciation in Iceland, *Geochem. Geophys. Geosyst.*, *3*(11), 1062, doi:10.1029/2001GC000282.

Mahoney, J. J., J. M. Sinton, M. D. Kurz, J. D. Macdougall, K. J. Spencer, and G. W. Lugmair (1994), Isotope and trace element characteristics of a super-fast spreading ridge: East Pacific Rise, 13°–23°S, *Earth Planet. Sci. Lett.*, *121*, 173–193.

McDougall, I., K. Sæmundsson, H. Jóhannesson, N. D. Watkins, and L. Kristjánsson (1977), Extension of the geomagnetic polarity time scale to 6.5 m. y.: K-Ar dating, geological and paleomagnetic study of a 3,500-m lava succession in western Iceland, *Geol. Soc. Am. Bull.*, *88*, 1–15.

Meyer, P. S., H. Sigurdsson, and J.-G. Schilling (1985), Petrological and geochemical variations along Iceland's neovolcanic zones, *J. Geophys. Res.*, *90*, 10,043–10,072.

O'Nions, R. K., R. J. Pankhurst, and K. Grönvold (1976), Nature and development of basalt magma sources beneath Iceland and Reykjanes Ridge, *J. Petrol.*, *17*, 315–338.

Óskarsson, N., S. Steinthorsson, and G. E. Sigvaldason (1985), Iceland geochemical anomaly: Origin, volcanotectonics, chemical fractionation and isotope evolution of the crust, *J. Geophys. Res.*, *90*, 10,011–10,025.

Pálmason, G. (1981), Crustal rifting, and related thermomechanical processes in the lithosphere beneath Iceland, *Geol. Rundsch.*, *70*, 244–260.

Perfit, M. R., and W. W. Chadwick Jr. (1998), Magmatism at mid-ocean ridges: Constraints from volcanological and geochemical investigations, in *Faulting and Magmatism at Mid-Ocean Ridges*, *Geophys. Monogr. Ser.*, vol. 106, edited by W. R. Buck et al., pp. 59–115, AGU, Washington, D. C.

Piper, J. D. A. (1973), Volcanic history and tectonics of the north Langjökull region, central Iceland, *Can. J. Earth Sci.*, *10*, 164–179.

Richter, D. H., J. P. Eaton, K. J. Murata, W. A. Ault, and H. L. Krivoy (1970), Chronological narrative of the 1959–1960 eruption of Kilauea Volcano, Hawaii, *U.S. Geol. Surv. Prof. Pap.*, *537-E*, 1–73.

Rossi, M. J. (1996), Morphology and mechanism of eruption of postglacial shield volcanoes in Iceland, *Bull. Volcanol.*, *57*, 530–540.

Rossi, M. J., and G. E. Sigvaldason (1996), The morphology and formation of flow-lobe tumuli on Icelandic shield volcanoes, *J. Volcanol. Geotherm. Res.*, *72*, 291–308.

Rowland, S. K., and G. P. L. Walker (1990), Pahoehoe and aa in Hawaii: Volumetric flow rate controls the lava structure, *Bull. Volcanol.*, *52*, 615–628.

Sæmundsson, K. (1962), Das Alter der Nesja-lava (SW Island), *Neues Jarb. Geol. Paleontol.*, *12*, 650.

Sæmundsson, K. (1966), Zwei neue C14–Datierungen isländischer Vulkanausbrüche, *Eiszeitalter Gegenwart*, *17*, 85–86.

Sæmundsson, K. (1974), Evolution of the axial rifting zone in northern Iceland and the Tjornes Fracture Zone, *Geol. Soc. Am. Bull.*, *85*, 495–504.

Sæmundsson, K. (1978), Fissure swarms and central volcanoes of the neovolcanic zones of Iceland, in *Crustal Evolution in Northwestern Britain and Adjacent Regions*, edited by D. R. Bowes and B. E. Leake, *Geol. J.*, *10*, spec. issue, 415–432.

Sæmundsson, K. (1979), Outline of the geology of Iceland, *Jökull*, *29*, 7–28.

Sæmundsson, K. (1990), Landsigid vid nordanvert Thingvallavatn 1789 (The subsidence of the northern shore of Thingvallavatn in 1789), in *Brunnur Lifandi Vatns*, pp. 90–96, Háskóli Íslands, Háskólaútgafan, Iceland.

Sæmundsson, K. (1992), Geology of the Thingvallavatn area, *Oikos*, *64*, 40–68.

Sæmundsson, K. (1995), Hengill geological map (bedrock), 1:50,000, Orkustofnun, Hitaveita Reykavikur and Landmælingar Íslands, Orkustofnun, Reykjavík.

Sæmundsson, K., and S. Einarsson (1980), Geologic map of Iceland, sheet 3, S-West Iceland, 2nd ed., Mus. of Nat. Hist. and Iceland Geod. Surv., Reykjvík.

Sæmundsson, K., and G. Ó. Friðleifsson (2001), Geological and geothermal maps of Torfajökull area Orkustofnun, *Rep. OS-2001/036*, 118 pp. and maps, Orkustofnun, Reykjavík.

Sæmundsson, K., and H. Jóhannesson (1994), Jarðlög upp af Síðu og Fljótshverfi, aldur og myndunarsaga (Build up and age of the rock sequence of the Síða-Fljótshverfi highland), paper presented at Geoscience Society of Iceland Spring Meeting, Reykjavík.

Schilling, J.-G. (1973a), Iceland mantle plume, *Nature*, *246*, 141–143.

Schilling, J.-G. (1973b), Iceland mantle plume: Geochemical evidence along the Reykjanes Ridge, *Nature*, *242*, 565–571.

Schilling, J.-G., P. S. Meyer, and R. H. Kingsley (1982), Evolution of the Iceland hotspot, *Nature*, *296*, 313–320.

Schilling, J.-G., M. Zajac, R. Evans, T. Johnston, W. White, J. O. Devine, and R. Kingsley (1983), Petrologic and geochemical variations along the Mid-Atlantic Ridge from 29°N to 73°N, *Am. J. Sci.*, *283*, 510–586.

Sigvaldason, G. E., K. Annertz, and M. Nilsson (1992), Effect of glacier loading/deloading on volcanism: Postglacial volcanic production rate of the Dyngjufjoll area, central Iceland, *Bull. Volcanol.*, *54*, 385–392.

Sinton, J. M., and R. S. Detrick (1992), Mid-ocean ridge magma chambers, *J. Geophys. Res.*, *97*, 197–216.

Sinton, J. M., S. M. Smaglik, J. J. Mahoney, and K. C. Macdonald (1991), Magmatic processes at superfast spreading mid-ocean ridges: Glass compositional variations along the East Pacific Rise, 13°–23°S, *J. Geophys. Res.*, *96*, 6133–6155.

Sinton, J., E. Bergmanis, K. Rubin, R. Batiza, T. K. P. Gregg, K. Grönvold, K. C. Macdonald, and S. M. White (2002), Volcanic eruptions on mid-ocean ridges: New evidence from the superfast spreading East Pacific Rise, 17°–19°S, *J. Geophys. Res.*, *107*(B6), 2115, doi:10.1029/2000JB000090.

Slater, L., M. Jull, D. McKenzie, and K. Grönvold (1998), Deglaciation effects on mantle melting under Iceland: Results from the northern volcanic zone, *Earth Planet. Sci. Lett.*, *164*, 151–164.

Stuiver, M. (1980), Workshop on $^{14}C$ data reporting, *Radiocarbon*, *22*, 964–966.

Stuiver, M., and H. A. Polach (1977), Discussion: Reporting of $^{14}C$ data, *Radiocarbon*, *19*, 355–363.

Stuiver, M., and P. J. Reimer (1993), Extended $^{14}C$ database and revised CALIB radiocarbon calibration program, *Radiocarbon*, *35*, 215–230.

Sun, S. S., and W. F. McDonough (1989), Chemical and isotopic systematics of ocean island basalts: Implications for mantle composition and processes, in *Magmatism in the Ocean Basins*, edited by A. D. Saunders and M. J. Norry, *Geol. Soc. Spec. Publ.*, *42*, 313–345.

Taylor, B., K. Crook, and J. Sinton (1994), Extensional transform zones and oblique spreading centers, *J. Geophys. Res.*, *99*, 19,707–19,718.

Thirlwall, M. F., M. A. M. Gee, R. N. Taylor, and B. J. Murton (2004), Mantle components in Iceland and adjacent ridges investigated using double-spike Pb isotope ratios, *Geochim. Cosmochim. Acta*, *68*, 361–386.

Thirlwall, M. G. (1995), Generation of the Pb isotopic characteristics of the Iceland plume, *J. Geol. Soc. London*, *152*, 991–996.

Thorarinsson, S. (1979), Tephrachronology and its application in Iceland, *Jökull*, *29*, 33–36.

Thorarinsson, S., S. Steinthorsson, T. Einarsson, H. Kristannsdóttir, and N. Óskarsson (1973), The eruption on Heimaey, Iceland, *Nature*, *241*, 372–375.

Thordarson, T., and Á. Hoskuldsson (2002), *Iceland*, *Classic Geology in Europe*, vol. 3, 200 pp., Terra Publishing, Harpenden, Hertforshire, UK.

Thordarson, T., S. Self, N. Óskarsson, and T. Hulsebosch (1996), Sulfur, chlorine, and fluorine degassing and atmospheric loading by the 1783–1784 AD Laki (Skaftár Fires) eruption in Iceland, *Bull. Volcanol.*, *58*, 205–225.

Thordarson, T., S. Self, D. J. Miller, G. Larsen, and E. G. Vilmundardóttir (2003), Sulphur release from flood lava eruptions in the Veidivötn, Grímsvötn and Katla volcanic systems, Iceland, *Volcanic Degassing*, in edited by C. Oppenheimer, D. M. Pyle, and J. Barclay, *Geol. Soc. Spec. Publ.*, *213*, 103–121.

Thors, K. (1992), Bedrocks, sediments and faults in Thingvallavatn, *Oikos*, *64*, 69–79.

Torfason, H., Á. Hjartarson, H. Jóhannesson, J. Jónsson, and K. Sæmundsson (1999), Geological map, bedrock geology, Vífilsfell 1613 III SA-B, 1:25000, Iceland Geod. Surv., Reykjavík.

Tryggvason, T. (1943), Das Skjaldbreid-Gebiet auf Island, Eine petrographische Studie, *Bull. Geol. Inst. Univ. Uppsala*, *30*, 273–320.

Unni, C. K., and J.-G. Schilling (1978), Cl and Br degassing by volcanism along the Reykjanes ridge and Iceland, *Nature*, *272*, 19–23.

Vergniolle, S., and C. Jaupart (1986), Separated two-phase flow and basaltic eruptions, *J. Geophys. Res.*, *91*, 12,842–12,860.

Vilmundardóttir, E., and G. Larsen (1986), Productivity pattern of the Veidivötn fissure swarm, southern Iceland, in postglacial times: Preliminary results, paper presented at the 17th Nordiska Geologmötet, Helsingsfors Univ., Helsinki.

Walker, G. P. L. (1965), Some aspects of Quaternary volcanism in Iceland, *Trans. Leicester Literary Philos. Soc.*, *59*, 25–40.

Walker, G. P. L. (1971), Compound and simple lava flows and flood basalts, *Bull. Volcanol.*, *35*, 579–590.

Walker, G. P. L. (1991), Structure and origin by injection of lava under surface crust of tumuli, "lava rise pits", and "lava inflation clefts" in Hawaii, *Bull. Volcanol.*, *53*, 546–558.

Wilson, L., and J. W. Head (1981), Ascent and eruption of basaltic magma on the earth and the moon, *J. Geophys. Res.*, *86*, 2971–3001.